

University of New Hampshire
University of New Hampshire Scholars' Repository

Master's Theses and Capstones

Student Scholarship

Winter 2009

Enzymatic reactions in microdevices

Michael O'Connor

University of New Hampshire, Durham

Follow this and additional works at: <https://scholars.unh.edu/thesis>

Recommended Citation

O'Connor, Michael, "Enzymatic reactions in microdevices" (2009). *Master's Theses and Capstones*. 516.
<https://scholars.unh.edu/thesis/516>

This Thesis is brought to you for free and open access by the Student Scholarship at University of New Hampshire Scholars' Repository. It has been accepted for inclusion in Master's Theses and Capstones by an authorized administrator of University of New Hampshire Scholars' Repository. For more information, please contact nicole.hentz@unh.edu.

ENZYMATIC REACTIONS IN MICRODEVICES

BY

Michael O'Connor

B.S. in Chemical Engineering, University of New Hampshire, 2006

THESIS

Submitted to the University of New Hampshire
in partial fulfillment of
the requirements for the degree of

Master of Science

in

Chemical Engineering

December 2009

UMI Number: 1481719

All rights reserved

INFORMATION TO ALL USERS

The quality of this reproduction is dependent upon the quality of the copy submitted.

In the unlikely event that the author did not send a complete manuscript and there are missing pages, these will be noted. Also, if material had to be removed, a note will indicate the deletion.



UMI 1481719

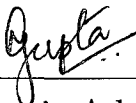
Copyright 2010 by ProQuest LLC.

All rights reserved. This edition of the work is protected against unauthorized copying under Title 17, United States Code.



ProQuest LLC
789 East Eisenhower Parkway
P.O. Box 1346
Ann Arbor, MI 48106-1346

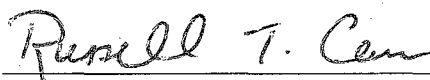
This thesis has been examined and approved.



Thesis Advisor, Dr. Nivedita R. Gupta
Associate Professor of Chemical Engineering



Co-Advisor, Dr. Palligarnai T. Vasudevan
Professor and Chair of Chemical Engineering



Dr. Russell Carr
Professor of Chemical Engineering

December 14, 2009

Date

DEDICATION

For Mom, Dad, Tom, David, and Meg, and the rest of my friends and family who have been so supportive of all my endeavors.

ACKNOWLEDGMENTS

I thank my thesis advisor, Dr. Nivedita Gupta, and my co-advisor, Dr. P.T. Vasudevan, whose support and encouragement have been invaluable to me in my graduate work. Mr. Jonathan Newell has graciously provided assistance and advice in many aspects of the fabrication and preparation of the equipment used for this work. I thank Eric Beauregard for his help in developing and implementing the procedures for fabricating microchannel devices. I also thank Dr. Russell Carr for serving on my thesis committee.

CONTENTS

DEDICATION	iii
ACKNOWLEDGMENTS	iv
LIST OF TABLES	vii
LIST OF FIGURES	ix
ABSTRACT	xiii
1 INTRODUCTION	1
1.1 Motivation	1
1.2 Objectives	5
2 BACKGROUND	8
2.1 Microdevice Fabrication	8
2.2 Hydrogen Peroxide Decomposition Reaction	11
2.3 Bovine Liver Catalase	12
2.4 Macroscale Enzyme Reactors	15
2.5 Microscale Enzyme Reactors	18
2.6 Kinetic Studies in Enzyme Microreactors	20
3 EXPERIMENTAL	24
3.1 Materials	24
3.2 Microdevice Fabrication	24
3.2.1 Silicon Master Mold	24

3.2.2	Inlet and Outlet ports	26
3.2.3	Casting and Sealing	27
3.2.4	Interfacing	29
3.2.5	Reactor Designs	30
3.3	Enzymatic Reactions in Microdevices	31
3.3.1	Free Catalase Reaction	33
3.3.2	Enzyme Immobilization on Microdevice Wall	34
3.3.3	Carrier-free Enzyme Aggregate Reaction	36
3.4	Analysis Techniques	39
3.4.1	Measurement of Channel Dimensions	39
3.4.2	Sample Collection	40
3.4.3	Measurement	40
4	RESULTS AND DISCUSSION	43
4.1	Microdevice Fabrication	43
4.1.1	Effect of Photomask Resolution	44
4.1.2	Effect of Rotation Under UV Lamp	45
4.1.3	Master Mold Fabrication Procedure	48
4.2	Enzymatic Reactions in Microdevices	52
4.2.1	Free Catalase Reaction	56
4.2.2	Enzyme Immobilization on Microdevice Wall	62
4.2.3	Carrier-free Enzyme Aggregate Reaction	65
5	SUMMARY AND FUTURE WORK	70

REFERENCES

74

APPENDIX A

77

LIST OF TABLES

3.1	Average device dimensions for designs listed in Figure 3-4. Error indicates largest variation between average and measured values. . . .	31
3.2	The experimental conditions used to conduct the free catalase reactions.	34
3.3	Experimental conditions used for experiments with immobilization of enzyme to the microdevice wall.	36
3.4	Device and treatment conditions used for experiments with immobilization of enzyme to the microdevice wall. Concentration (C) is in v/v% for 3-APTES and Glutaraldehyde and in U/mL for the enzyme treatment. Flowrate (F) has units of $\mu\text{L}/\text{min}$ and time (T) has units of hours.	37
3.5	Experimental conditions used for carrier-free enzyme aggregate reactions.	39
3.6	Dripping rate for the drops exiting the microdevice for carrier-free enzyme aggregate experiments.	41
4.1	Effect of changing certain process parameters on the silicon master mold fabricated.	44
4.2	Dimensions in μm of the microfluidic channels fabricated from three master molds fabricated from the same photomask of $100\mu\text{m}$ width. .	51
4.3	Comparison of design and fabricated width for patterns used in this research. Average values are shown for fabricated width. Error indicates largest variation between average and measured values. . . .	51
4.4	Parameters for calculation of total enzyme exposed to channel walls during treatment. Protein concentration provided by manufacturer. .	64

4.5 Parameters used for calculation of observed activity and total enzyme present.	65
---	----

LIST OF FIGURES

3-1	Schematic of the master mold fabrication process.	26
3-2	Casting and sealing procedure for microchannels.	28
3-3	Procedure for interfacing the microchannels with macroscale equipment.	30
3-4	Channel designs used in the enzymatic reaction experiments.	31
3-5	Schematic of the experimental apparatus for the carrier-free enzyme aggregate reactions.	33
3-6	Standard calibration curve for hydrogen peroxide at a wavelength of 240 nm.	42
4-1	SEM images of PDMS layers cast from a stamp that was made using a (a)-(c) 5,000 dpi resolution photomask, and a (d)-(f) 20,000 dpi resolution photomask.	46
4-2	Cross-sectional images from three locations on a PDMS microdevice cast from a mold made using a 20,000 dpi photomask.	47
4-3	Dimensions in μm along the length of the microfluidic channel fabri- cated (a) with and (b) without rotation under the UV lamp.	49
4-4	Flow patterns with (a) slug flow and (b) parallel flow possible in the microdevices.	53
4-5	Model reactor series scheme to analyze the microdevices in this research.	54
4-6	Evolution of substrate concentration with residence time for the model problem with $[S]_0 = 30$ mmol/L, $v_{max} = 6$ mmol/L-min, $K_M = 35$ mmol/L, $\tau_{PFR} = 2$ min, and $\tau_{FB} = 1.25$ min.	57

4-7	Effect of v_{max} on $[S]_0 - [S]_f/\tau_{TOT}$ as a function of initial substrate concentration $[S]_0$. $K_M = 35$ mmol/L, $\tau_{PFR} = 2$ min, and $\tau_{FB} = 1.25$ min.	58
4-8	Effect of K_M on $[S]_0 - [S]_f/\tau_{TOT}$ as a function of initial substrate concentration $[S]_0$. $v_{max} = 6$ mmol/L-min, $\tau_{PFR} = 2$ min, and $\tau_{FB} = 1.25$ min.	59
4-9	Average reaction rate as a function of initial substrate concentration in the absence and presence of a fed batch reactor with $v_{max} = 6$ mmol/L-min, $K_M = 35$ mmol/L, $\tau_{PFR} = 2$ min, and $\tau_{FB} = 1.25$ min.	60
4-10	Initial reaction rate results for the decomposition of hydrogen peroxide by a solution of 6 U/mL and 12 U/mL of bovine liver catalase in a PDMS microdevice. Design features and reaction conditions correspond to experimental conditions A1 and A2 in Table 3.2.	61
4-11	Average reaction rate versus initial substrate concentration for experiments with enzyme immobilization on microdevice walls for the conditions specified in Table 3.4.	63
4-12	Average reaction rate versus initial substrate concentration for experiments with enzyme immobilization on microdevice walls for using the conditions specified in Table 3.4. Data points in both B1 series were taken starting at low initial substrate concentrations and progressing higher. In the B2 series, data collection started with a high initial substrate concentration and progressed to lower amounts.	64
4-13	Image of two cross-linked catalase aggregate particles at 40x magnification. This image was taken prior to filtration.	66
4-14	Initial reaction rate as a function of the initial substrate concentration for two batches with enzyme aggregates using diglyme and acetone as precipitants in the formation of the cross-linked enzyme aggregates.	67

4-15 Lineweaver-Burk plot of batch reactions using diglyme precipitated aggregates.	68
4-16 Average reaction rate as a function of initial substrate concentration for carrier-free enzyme aggregate reaction conditions shown in Table 3.5.	69

ABSTRACT

ENZYMATIC REACTIONS IN MICRODEVICES

by

Michael O'Connor

University of New Hampshire, December, 2009

Enzyme reactions conducted in microdevices for diagnostic applications minimize the enzyme usage. In this research, polydimethylsiloxane microdevices were fabricated and used to study the well studied hydrogen peroxide decomposition reaction using bovine liver catalase. Soft lithography techniques were developed to fabricate custom-made microdevices in-house. High resolution photomasks and oxygen plasma treatment followed by baking for 2 – 3 hours yielded microdevices with vertical walls that did not leak easily. Flow experiments were conducted with free enzyme, enzyme immobilized on microdevice walls, and carrier-free enzyme aggregates. For free enzyme and carrier-free enzyme aggregate reactions, the average reaction rate showed a maxima at ~ 80 mmol/L as predicted from macroscale batch experiments. The trend for average reaction rate was consistent with the model series reactor scheme developed. Covalent binding of enzyme to the microdevice wall was not achieved as the enzyme was found to continuously leach from the microdevice walls.

CHAPTER 1

INTRODUCTION

1.1 Motivation

Enzymes have found use in industrial applications due to their specificity and ability to catalyze reactions at less extreme temperatures and pressures than many traditional inorganic catalysts. This is beneficial since milder conditions can lower operating costs and increase safety. Detergents represent one of the largest industrial uses of enzymes where proteases and amylases are used to remove protein and starch stains. They have also been used extensively in the food and beverage industries for the removal of lactose from dairy products, the maturation of beer, and the strengthening and whitening of bread dough [18]. Other uses include wastewater treatment [7], production of semi-synthetic penicillins[30], and processing of leather as well as many others [15]. Enzymes are chains of amino acids that have several levels of structure. These levels of structure describe the sequence of amino acids (primary structure), common three dimensional shapes that certain sequences form (secondary structure), the specific orientation in space that the amino acid chain takes when fully formed (tertiary structure), and the overall physical orientation of all subunits

(quaternary structure, for those enzymes with multiple subunits). Enzyme function is frequently dependent on maintaining the native conformation. Enzymes are a class of proteins that catalyze chemical reactions with a high degree of specificity. They act on very specific substrates and produce very specific, often enantiomerically pure, products. Traditional methods using inorganic catalysts are not as selective in the products they produce which often leads to racemic mixtures. This specificity can reduce the complexity and cost of production for many chemicals as compared to traditional methods, particularly those requiring high enantiomeric purity. By producing a pure product, undesired by-product streams are eliminated, resulting in less waste and reducing environmental impact. Examples of this include the production of L-Aspartic acid from fumaric acid, resolution of enantiopure alcohols from racemic mixtures, and production of R-Mandelic acid from racemic mandelonitrile [30]. However, enzymes are often very expensive and many are easily damaged by heat or pH changes. Small quantities of enzyme are often very expensive and separating free enzyme from a solution is generally very difficult. One simple way to keep costs down is to use smaller quantities of enzyme in testing applications, such as the common bioassay ELISA. Exposure to high heat or extreme pH can render an enzyme inactive by denaturing, or unfolding, its delicate three dimensional structure [46]. Immobilization of enzymes can add to their stability over wider temperature and pH ranges and also allow for their recovery and reuse [33].

Microfluidic reactors are devices that contain flow channels or chambers ranging from several hundred microns to single micron dimensions [48]. Traditional macroscale reactions, even when scaled down greatly, require a large amount of reactant compared to microfluidic reactors. Their ability to use smaller sample sizes

can decrease the total diagnostic time and reduce overall chemical waste streams in addition to an overall reduction in cost. Photolithography is the most successfully implemented microfabrication technology, finding extensive use in the semiconductor industry. It generally requires a clean room and significant capital investment for the required equipment. Fabrication has also been completed using techniques such as micromachining of silicon and glass. The production cost of these micromachined surfaces is very high and significant capital investment and expertise are required. Wet etching with caustic chemicals has also been used for the creation of microstructures. These micromachined surfaces are combined with techniques such as hot embossing to create microchannels in plastic surfaces. Hot embossing relies on high temperature and pressure to leave the imprint of a desired pattern in the plastic surface. Further developments in microdevice fabrication, particularly by the Whitesides research group, have led to a set of techniques referred to as soft lithography [48, 50]. In this technique a master mold is produced using a substrate, often silicon, and a photoresist, which is a chemical that polymerizes upon exposure to UV light. Removal of the unexposed photoresist provides a patterned master mold. Soft lithography then uses an elastomer like polydimethylsiloxane (PDMS) to make microdevices rapidly and without a large capital investment compared to other miniaturization technologies. PDMS is a preferred material for soft lithography because it is non-toxic, cures at low temperatures, can reproduce micron-sized features very reliably, and can be sealed reversibly or irreversibly.

Microfluidic devices provide the opportunity to accomplish miniaturization for enzyme reaction applications to minimize enzyme use, specifically for diagnostic applications. The use of enzymes within microdevices complements the strengths of

these two fields. Considering these potential benefits, the effect that a microscale environment may have on enzyme kinetics is of great interest. Microfluidic devices have been used to conduct screening for protein crystallization [14, 52], microscale enzyme linked immunosorbent assay (ELISA) [20], and cell sorting [11]. Each of these examples provide a significant reduction in the volume of reagent used and thus represent a potential reduction in assay cost. Hansen et. al. [14] formed devices with dead-end channels to rapidly screen protein crystallization conditions. They observed faster crystallization times in the microdevice than with traditional macroscale experiments. Crystals grew large enough in their microdevice for X-ray diffraction studies. Zheng et. al. [52] formed protein crystals in microchannels by creating an array of droplets with varying concentrations of protein and precipitant. This method decreased each trial volume by approximately one order of magnitude. These droplets were smoothly transferred intact to a connected glass capillary and diffraction studies performed on crystals formed in these drops. Both methods demonstrate a significant cost and time savings in screening for crystallization conditions. ELISA is a detection assay to determine the presence of antibodies or antigens in a sample. Normally performed in microtiter plates, it has been performed in microchannels [9], and demonstrated comparable detection sensitivity. That study also demonstrated a common problem of non-specific protein adsorption on PDMS. This challenge was overcome by a combination of surface modification and blocking solutions. The use of microdevices for cell sorting has shown it as viable, though slower than traditional methods. It does offer the prospect of a disposable device which eliminates the need for cleaning and sterilization, and the risk of contamination from previous runs [11].

1.2 Objectives

The objective of this work is to develop soft lithography techniques to fabricate custom-made microfluidic devices to conduct enzymatic reactions at the microscale. Furthermore, different strategies to conduct enzyme reactions in microdevices are investigated. Flow reactions using free enzyme and substrate are the simplest starting point for integration of microfluidics and enzyme kinetics. Since enzymes, as catalysts, are not consumed by the reactions they affect, the opportunity to reuse them is very appealing due to their high cost. Immobilization is one approach that allows reuse and can be accomplished in several ways. Binding the enzyme to the channel wall eliminates the need for a separation process after completion of the reaction. It often reduces activity compared with the free enzyme and can be challenging to accomplish. Eliminating the carrier by binding the enzyme to itself maintains high activity levels but does require a separation process after the reaction is complete. The objectives of this study are:

- **Microdevice Fabrication using Soft Lithography:** Develop soft lithography techniques to fabricate custom-made microdevices. These devices provide a platform for kinetics studies on the microscale and do not require the specialized conditions or equipment necessary for other photolithography techniques. These studies are a first step in understanding the challenges of fabricating miniaturized multi-step chemical processing devices, commonly referred to as lab-on-a-chip devices, which are intended for use as fast and portable chemical analysis and processing devices.
- **Enzymatic Reactions in Microdevices:** Conduct enzymatic reactions in

microdevices using a well understood hydrogen peroxide decomposition reaction using the enzyme catalase. Different strategies exist for conducting enzymatic reactions in microdevices. Flow reactions were the simplest to implement but did not allow for separation of the enzyme for reuse. Immobilization of enzyme on the channel wall as well as fabrication of enzyme aggregates by cross-linking allow for easy separation of enzyme.

The kinetics and physics of flow on the microscale differs from the macroscale as different forces become dominant. The ratio of surface area to volume increases greatly on the microscale, often by several orders of magnitude [50]. The Reynolds number describes the type of flow present in a pipe or channel and is given as

$$Re = \frac{\rho v D_h}{\mu} \quad (1.1)$$

where ρ is the density of the fluid, v is the velocity of the fluid, D_h is the hydraulic diameter and μ is the viscosity of the fluid. When $Re < 2300$, the expected flow type is laminar for flow in a circular pipe. Above that value, turbulent flow can be expected. In microfluidic devices, flow is almost exclusively laminar, which limits mixing primarily to diffusion. This can become the rate limiting step due to the speed of many enzyme reactions. Several methods have been developed that rely on channel geometry such as serpentine channels [36] and surface conditions to induce chaotic advection or fluid folding to hasten mixing [38, 52]. These features increase mixing of separate fluid streams within microdevices.

Immobilization is an important procedure for enzyme recovery in biochemical reactions. There are a variety of enzyme immobilization methods available but each

method has certain drawbacks. Physical adsorption is one of the simplest methods but has problems with stability over time. Entrapment is another method which has been implemented. This can require additional skill in fabrication and may denature the enzyme during formation. Some entrapment methods also require specific chemistries which are not available for all enzymes [26]. Binding an enzyme to a carrier allows for reuse but the overall enzyme to carrier mass ratio can become very small. Immobilization by carrier-free methods eliminates this problem but creates the need for an additional separation process if the enzyme is to be reused. Fabrication methods, particularly some surface treatments for sealing microchannels, can denature enzymes and thus, certain immobilization procedures must be completed after this step.

CHAPTER 2

BACKGROUND

2.1 Microdevice Fabrication

The most developed method for microfabrication is photolithography. It has been used extensively in the fabrication of microprocessors. This technology uses a projected image to create a pattern on a photoresist layer on the surface of a silicon wafer. Photolithography requires the use of a clean room and specialized equipment for producing, scaling, and projecting the reticle image on the photoresist. This represents a significant capital investment for a lab to implement this method of microstructure fabrication [50]. Other methods include micromachining of silicon and glass surfaces. These techniques also require significant capital investment and additional expertise. Alternatives have been developed that reduce the need for expensive equipment and technical skill. Soft lithography is a set of techniques that have been largely developed and refined by the Whitesides research group [29, 48, 50]. It provides alternative methods of microfabrication that avoid some of the drawbacks of photolithographic techniques. Specifically, it eliminates the need for high-energy radiation and significant capital investment in equipment, provides the opportunity to

use a wider variety of materials, and allows for many surface chemistry modifications. It can also rapidly produce prototypes on the micrometer scale [50]. Collectively, soft lithography refers to the following techniques: microcontact printing (μ CP), microtransfer molding (μ TM), micromolding in capillaries (MIMIC), solvent-assisted micromolding (SAMIM), and replica molding (REM).

Soft lithography techniques involve the creation of a master mold using photolithography combined with printed photomasks designed using computer aided drafting (CAD) software. A polished silicon wafer is coated with a photoresist. The thickness and uniformity of this layer are controlled by the combination of photoresist viscosity and spin coating parameters such as rotational speed and time. This photoresist is polymerized in the presence of UV light. The resolution of the master mold is dependent upon the resolution of the photomask and the angle of exposure to the UV light source. By designing a two-dimensional photomask and controlling the thickness of the photoresist by spin-coating, a three dimensional raised pattern can be created after developing the photoresist. Development removes unpolymerized photoresist leaving the desired pattern. This procedure requires minimal equipment: a UV light source, oven, and spin coater. This master mold is the starting point for each of the techniques listed above.

Microcontact printing Microcontact printing (μ CP) is a straight-forward concept analogous to using a rubber stamp with ink to replicate a pattern. Polydimethylsiloxane (PDMS), a silicone elastomer, has frequently been used in soft lithography techniques due to its physical and chemical properties. It is transparent, elastic, homogeneous, and its surface can easily be modified by oxidation [50]. This viscous

liquid can be poured over the photoresist/silicon mold and cured slowly at room temperature or more quickly by heating. Upon fully curing, the PDMS layer can be peeled off the master, leaving an imprint of the raised master mold pattern in its surface. The master mold is cast using PDMS or a different flexible silicone rubber. A self-assembled monolayer can be formed on the patterned polymer surface and these molecules can then be transferred to a desired substrate in a very specific pattern.

Microtransfer molding Microtransfer molding (μ TM) uses the same method of creating a master mold and casting a polymer slab. After removing this slab from the master, the spaces are filled with a liquid precursor and placed on a substrate and the prepolymer is cured. Removal of the polymer slab leaves a patterned surface.

MIMIC & SAMIM MIMIC is similar to μ TM but the polymer slab is placed on the substrate and prepolymer is drawn into microchannels by capillary action. SAMIM begins the same way as μ TM, casting a polymer layer from the master mold. A second polymer, which will form the final structure, is chosen. The cast layer is removed from the master mold and a solvent is applied. This cast layer is placed in conformal contact with the second polymer. The solvent swells this layer, forming it to the spaces in the cast polymer layer. The solvent evaporates, leaving the final structure intact.

Replica molding Replica molding (REM) also begins with casting a polymer using the master mold. By exposing this layer and a flat layer (PDMS, glass slide, etc.) to plasma, the two layers can be irreversibly bound together, forming a sealed microchannel network. The plasma exposure replaces the methyl ($-CH_3$) groups

normally found on the surface with hydroxyl (-OH) groups. This alters the surface properties, making the PDMS temporarily hydrophilic. This chemistry will revert back to its native state over time, returning the surface to a hydrophobic state [35]. Reversible seals are possible using a material such as PDMS, which can form a conformal seal to another flat layer. These seals are significantly weaker than the plasma bonding method and thus are suitable only for certain applications. PDMS has been used to create a wide array of devices that scale down traditional macroscale assays. This technology has provided the foundation for a vast array of applications.

2.2 Hydrogen Peroxide Decomposition Reaction

The breakdown of hydrogen peroxide is important in many organisms. Aerobic processes in many cells produce hydrogen peroxide which is toxic to the cell itself. These cells survive due to the presence of enzymes such as catalase and peroxidase which quickly remove hydrogen peroxide, leaving the harmless products of water and oxygen gas [12]. Hydrogen peroxide is a naturally existing chemical that breaks down slowly over time in the following reaction:



Without the presence of a catalyst, the activation energy for this reaction is approximately 71 kJ/mol. Catalysts, which function by reducing the activation energy necessary for the reaction to occur, can greatly increase the rate of reaction. A comparison of catalase and traditional catalysts demonstrates this effect [47]. This

reaction can be catalyzed by inorganic catalysts such as hydrogen bromide (HBr) or iron salts (Fe^{+2} , Fe^{+3}), and by enzymes such as catalase or peroxidase. The breakdown of hydrogen peroxide takes place at a rate of approximately 10^{-8} M/s in the absence of a catalyst. In the presence of hydrogen bromide, this rate increases to approximately 10^{-4} M/s. Iron salts increase the rate even further to 10^{-3} M/s. The catalyst $Fe(OH)_2TETA^+$ is significantly faster than both of these at 10^3 M/s. None are as active in the decomposition reaction as catalase. Catalase is much faster than any of these at a rate of approximately 10^7 M/s. With this catalyst, the activation energy is reduced to approximately 8 kJ/mol.

2.3 Bovine Liver Catalase

Enzymes are a class of molecules, frequently proteins, that catalyze chemical reactions. Their behavior is influenced by temperature, pH, and in many cases, the presence of inhibitors or cofactors. Structurally, they are extremely complex. Amino acids are the building blocks of enzymes. Enzyme functionality is highly dependent on an intricate folded three dimensional structure which can easily be destroyed by extreme temperatures and pH changes. They have increasingly found applications in a wide array of industries. Enzymes are made up of polypeptide structures. Each polypeptide is a sequence of amino acids. There are 20 common amino acids, which are the building blocks of proteins. These amino acids can be polar or non-polar and can have a net positive, neutral, or negative charge. The order in which these amino acids are arranged is referred to as the primary structure. Certain amino acid sequences form common three dimensional structures, such as the α -helix or

β -strand, which comprise the secondary structure. The three dimensional arrangement that these secondary structures take is referred to as the tertiary structure. In larger proteins, this tertiary structure may have several distinct subunits, called domains. Proteins are folded into a specific three dimensional structure containing all of its subunits. This final level of spatial orientation between the subunits is referred to as the quaternary structure. The structures discussed are primarily stabilized by hydrophobic interactions and hydrogen bonding between individual amino acids [43, 46].

Catalase is an enzyme present in many cells including mammalian, fungal, and bacterial cells. Its wide presence across many cell types and in many organisms was described in 1900 [22] and it was first crystallized in 1937 [40]. Its three dimensional structure was later described [27] and refined [10]. Common preparations of catalase are extracted from bovine liver or *Aspergillus niger*. Catalase from bovine liver is a multimeric enzyme with four subunits and can be modeled at low substrate concentrations using the Michaelis-Menten equation [5, 41] given by,

$$v_0 = \frac{v_{max}[S]}{K_M + [S]}. \quad (2.2)$$

Here, $[S]$ is the substrate concentration, v_0 is the initial rate of reaction, v_{max} is the maximum rate of reaction, and K_M is the Michaelis constant for the enzyme. K_M and v_{max} can be determined using the Lineweaver-Burke plot [21] where a linear regression is performed on experimental data for $1/v_0$ versus $1/[S]$ and v_{max} and K_M are determined from the slope and intercept values. When substrate concentrations are high, such that $K_M/[S] \ll 1$, the equation reduces to $v = v_{max}$. When substrate

concentrations are low, such that $K_M/[S] \gg 1$, the equation reduces to $v = \frac{v_{max}}{K_M} [S]$. Thus, Michaelis-Menten kinetics predicts a constant maximum reaction rate at high substrate concentrations and a linear relationship at low substrate concentrations. At high substrate concentrations, bovine liver catalase displays substrate inhibition [19]. The optimum pH for catalase was determined to be approximately 7 [6]. Switala and Loewen [41] have studied catalases from several sources. The experimental K_M value they report for bovine liver catalase is 93 mM. Catalase, the enzyme used in this thesis, has successfully been covalently bound to many substrates such as chitosan[2], magnesium silicate[44], eggshells [3], dextran [25], and glass [45]. These immobilization procedures primarily cover work on the macroscale. Catalase immobilized on chitosan, a natural polymer, was observed to have a maximum rate coefficient, v_{max} , about half that observed for the free enzyme. The Michaelis constant, K_M , was approximately the same for both. The immobilized enzyme, stored wet, had better storage properties than the free enzyme, with approximately 50% activity remaining compared with 25% activity remaining after 28 days [2]. Catalase immobilized to magnesium silicate was accomplished using glutaraldehyde to bind the enzyme to the substrate and using an additional spacer molecule (3-APTES) between the substrate and glutaraldehyde. The observed increase in the K_M values was attributed to possible diffusion limitations between the bulk fluid and a thin film environment surrounding the immobilized enzyme. The v_{max} values for immobilized enzyme decreased by 2 – 3 orders of magnitude compared to the free enzyme. Approximately 90% of the initial enzyme activity remained after 20 days for the method without the spacer molecule while approximately 30% remained for the method with the 3-APTES spacer after the same period [44]. Eggshells were used to immobilize catalase

by linking with glutaraldehyde. Improvements were observed in the storage stability with 96% activity remaining after 36 days at 5°C [3].

2.4 Macroscale Enzyme Reactors

Enzyme catalyzed reactions are necessary for many cellular processes and most commonly occur with the free enzyme in solution. This is the simplest method of employing an enzyme in a laboratory setting as well. Batch reactions using enzymes are simple to conduct and reaction conditions can be controlled with relative ease. Flow reactions can also be conducted using free enzyme. Mixing can be accomplished through turbulent flow or by diffusion during laminar flow. Free enzyme reactions have a significant drawback. Once the enzyme has dissolved in solution it cannot be readily reused. This can have a significant impact on the overall cost of the process. In order to avoid this, enzymes can be immobilized using several different methods. Immobilization of enzymes can improve their stability of larger temperature and pH ranges. Since enzymes catalyze reactions, and thus are not consumed, their high cost makes reuse desirable. Immobilization can allow for the reuse or recycling of enzymes. It is not without drawbacks though. Many immobilization methods achieve this stability and reuse at the expense of some activity as compared with free enzyme. Several different methods of enzyme immobilization exist and each is best suited to particular applications. These methods can be broken down into four groups: binding by adsorption, by covalent bond, by incorporation, and as aggregates.

Adsorption Immobilization by adsorption relies on weak forces, such as hydrophobic interaction and van der Waals forces, to bind the enzyme to a substrate surface. This method of binding has been successful in immobilizing enzymes on substrates but is too weak to be suitable for most industrial scale use [33]. It has been applied successfully in the Tanabe process using ionic adsorption to bind aminoacylase to modified cellulose. Lipase (CaLB) has been immobilized on porous acrylic and commercialized. One major drawback of adsorption as an immobilization method is the possible leaching of the enzyme, in which the adsorbed enzyme detaches from the substrate and enters the bulk solution as free enzyme [33].

Covalent Covalent bonds rely on the strong forces of a shared electron to bind molecules together rather than the weaker forces resulting from ionic and physical bonding methods. A primary benefit of covalent immobilization is the strength of the bond created. Leaching of the enzyme from the immobilized surface is generally not a concern when covalent binding is used. Various chemistries exist to form the bond. Covalent bonding has been used successfully to bind enzymes and other proteins to a variety of surfaces including glass, polymers, and metals. Silica and glass have been silanized using 3-aminopropyltriethoxysilane (3-APTES) and functionalized by attachment of glutaraldehyde or branched polyethyleneimine as a means of providing a covalent binding site for the enzyme [4]. Though covalent binding is the strongest method to attach an enzyme to a carrier, procedures for doing so often involve multiple steps and can be challenging to successfully complete. The choice of substrate limits which techniques are available based on functional groups at the surface. Silicone rubber has been modified to allow covalent attachment of thermophilic β -glycosidase

by silanization and glutaraldehyde treatment [42]. This resulted in slow reaction due to low surface loading of enzyme. The overall conversion of substrate reached a maximum of approximately 60%, though this may have been impacted by product inhibition. This same basic method was used with silicon and the enzyme trypsin [8]. Reproducibility was found to be poor in this system.

Monolithic Enzymes have been incorporated into the bulk phase material of some devices to create monoliths with the desired enzyme functionality. Sol-gel chemistries have been used extensively for monolithic immobilization of enzymes. The method of drying used has a large effect on the morphology of the final product [33]. A monolith structure was created and the enzyme trypsin was successfully covalently bound within the material. This was found to be a stable environment which allowed for a high throughput exceeding normal values for packed bed reactors [51]. This device also improved stability over a wider pH range, with a 10% increase in activity observed at pH 6.0 and a 62% increase at pH 10.0. The optimum pH for this enzyme is 8.0. Flowrates for this monolith correspond to approximately 400 mL/min in a standard 25 mm packed bed column. This is a throughput approximately 8 times higher than the recommended maximum from one manufacturer for a standard packed bed column.

Aggregate Two primary methods of enzyme aggregation are currently used for immobilization. Cross-linked enzyme crystals require crystallization using highly pure enzyme. The crystallization procedure can be difficult and expensive compared to the use of cross-linked enzyme aggregates. The creation of enzyme aggregate particles relies on precipitation of the enzyme from a solvent and subsequent binding

by glutaraldehyde. These particles stabilize the enzyme while maintaining high levels of activity compared to the free enzyme. In some cases, a higher activity has been observed in the aggregate particles than the free enzyme. Aggregates of lipase, phytase, galactose oxidase, glucose oxidase, and others have been produced using high-throughput methods [31, 34]. These aggregates retained a high level of activity and could be scaled up several orders of magnitude using similar reaction conditions. Choice of precipitant is an important factor in retaining the activity of the aggregate particle [31].

2.5 Microscale Enzyme Reactors

Flow reactors

Flow reactors can be operated using a continuous flow or a stopped-flow model. In stopped flow, the reactor is filled with a fluid and the flow is halted to achieve a specified residence time. At the end of the specified reaction time, flow is resumed and the reaction mixture is forced out of the reaction chamber. Continuous mode reactors rely on steady flow conditions to provide a desired residence time. Flow can be driven by electrophoresis, which relies on an imposed electrical field to influence ions in solution, or by a pressure drop. This pressure drop can take the form of a decreased pressure at the outlet to draw fluid through the reactor or an increase in pressure on the inlet side, forcing the fluid through the reactor. Syringe pumps are commonly used to drive flow in microreactors. Continuous flow microchannel reactors have been observed to increase the rate of enzymatic reactions compared with standard batch reactions [16].

Immobilized reactors

Microscale immobilized enzyme reactions can be conducted in microcapillary tubes made of glass or in microdevices made from a variety of polymers. PDMS is a polymer that has commonly been used to create homogeneous fluid flow channels with rectangular cross-sections. Channels with circular cross-sections have been fabricated using polymers cast around high gauge wire, which is then removed, leaving a channel for fluid to flow through. Hybrid devices, containing microchannels formed in PDMS and a rigid fourth wall have commonly been made by sealing a glass slide or coverslip to the polymer surface. Immobilization methods vary depending on substrate and include silanization of etched glass surfaces, binding biotin-enzyme compounds to streptavidin coated substrates [17], and entrapment within a hydrogel on a substrate surface. Nomura et. al. [28] have used magnetic microbeads to create flow reactors within PTFE tubes. Permanent magnets fixed in place outside the PTFE tubes held a magnetic particle bed in place within the tubing. Immobilization of glucose oxidase was accomplished using silanization and linking by glutaraldehyde on magnetic and non-magnetic silica gel beads. Measurements were taken electrochemically, though the system could also be adapted for optical measurements. Immobilization of the enzyme on the microbeads, and immobilization of the microbeads by magnets allows for minimal deadtimes between reaction bed and measurement. Storage of the enzyme-immobilized magnetic microbeads over a period of 8 months showed high stability. PikC hydroxylase has been immobilized on agarose beads containing Ni-NTA by incubation of the beads in an aqueous PikC solution [37]. These beads were used in a batch comparison to free enzyme in solution. The kinetic parameters were

observed to decrease, with v_{max}/K_M showing a 5x decrease, but the half-life of the enzyme under reaction conditions increased from approximately 3 – 9 hours.

2.6 Kinetic Studies in Enzyme Microreactors

Kinetic studies of enzyme reactions conducted in microchannels vary in their procedures and analysis of experimental data. Observed rates can be affected by mass transfer resistance leading to a variety of reported efficiencies in various studies. The large surface to volume ratio that exists in microchannels increases the importance of adsorption and desorption effects. Enzymes, as discussed earlier, rely on a specific three dimensional structure to remain active. Explanations for reduction in activity of immobilized enzymes include steric hindrance and conformational changes from the immobilization procedure.

Han et. al. [13] fabricated a microfluidic PDMS device to measure the kinetics of droplet-based enzyme reactions. These systems consisted of a bulk carrier fluid, silicone oil, and an aqueous drop containing the substrate and enzyme in solution. Measurements were based on amperometric measurements from integrated electrodes. Bovine liver catalase was used to decompose hydrogen peroxide. The analysis was carried out using Michaelis-Menten kinetics as a model. Variations in substrate concentration were accomplished by control of the aqueous solution flowrates. The reaction time was controlled using pneumatic valves to define a shorter or longer flow path through the channels of the device. The value obtained by Lineweaver-Burk plot for K_M was 62 mM which is consistent with published literature [41].

Kerby et. al. [17] conducted experiments using alkaline phosphatase bound to

biotin. A packed bed of streptavidin coated microspheres was created in a borosilicate glass chip. The biotin bound enzyme was immobilized by flowing through the packed bed in excess. Measurements were conducted by appearance of a fluorescent product molecule and concentrations were obtained using a standard curve created using the fluorescent product molecule in the device. Initial rate experiments were first conducted with the enzyme in solution. The turnover rate determined for the free enzyme was $484.8s^{-1}$. Flow experiments with the immobilized enzyme using four separate flowrates for initial rate experiments gave a K_M value of $51.75 \pm 5.22 \mu\text{M}$ and a k_{cat} of $17.67 s^{-1}$. The turnover rate was determined from the experimental v_{max} value by estimating an enzyme density on the bead surface. Using the parameter they propose for determining the importance of mass transfer limitations, the consistent K_M value is attributed to the minimal importance of mass transfer resistance. This is due to the slow reaction rate. The increase in K_M as compared to the free enzyme value is attributed to steric hindrance or deactivation as a result of the immobilization process. The reduction in k_{cat} is attributed inaccessibility of some enzyme to the substrate [17].

Seong et. al. [32] fabricated a continuous flow packed-bed microscale reactor to study immobilized horseradish peroxidase. The enzyme was immobilized on $15 \mu\text{m}$ streptavidin coated spheres via conjugation with biotin. The microdevice was fabricated using photolithography for the creation of a master mold and casting with PDMS. This layer and a glass slide were exposed to oxygen plasma and irreversibly sealed. The reaction was measured based on appearance of a fluorescent product. Their results show observed K_M values that vary with flowrate. This variation ranges from a K_M of $2.32 \mu\text{M}$ for a flowrate of $0.2 \mu\text{L}/\text{min}$ to a K_M of 13.0 for a flowrate of

1.5 $\mu\text{L}/\text{min}$. Calculation of the intrinsic K_M value was based on data extrapolated for a zero flow condition and was similar to the solution phase value. The zero flow condition was proposed as the value least affected by mass transfer resistance. This method of determining a value for K_M was based on the idea of mass transfer hindering the measure of intrinsic reaction rate. Kerby et. al. argue that increases in flowrate decrease mass transfer resistance by thinning the boundary layer near surfaces and thus, the zero flow condition would not be appropriate for minimizing the effect of mass transfer resistance. Additionally, comparison of the reaction rate to diffusion rate using the published details shows it is very likely that mass transfer limitations did not affect the system and do not explain the variation of K_M with flow rate.

Mao et. al. [24] studied immobilized alkaline phosphatase in a microreactor. This enzyme was immobilized on the channel walls of the borosilicate tubing and PDMS/glass hybrid devices using phosphotidylcholine, biotin, and streptavidin. The streptavidin formed a conjugate with the enzyme that bound to the biotin surface molecules. Initial rate experiments were carried out using a 300 second reaction time. Data collected were based on fluorescence measurements. The reaction rate constant, k_{cat} , was observed to be $60.6 \pm 9.4 \text{ s}^{-1}$. This is a six-fold decrease as compared to the bulk reaction k_{cat} of $365 \pm 69 \text{ s}^{-1}$. The proposed reasons for this difference in turnover rate were steric hindrance, immobilization chemistry, and enzyme conformation. It is likely that mass transfer resistance played a role in the observed decrease. An analysis using the parameter proposed by Kerby et. al. demonstrates this quantitatively.

Logan et. al. [23] created polymer monoliths in capillary channels. These monoliths were treated with PEG and vinyl azlactone to covalently bind horseradish peroxidase and glucose oxidase for kinetic studies. The reaction was measured by formation of a fluorescent product. Non-specific protein adsorption was successfully controlled through the inclusion of PEG and Tween-20 concentrations of 0.01 v/v%. Analysis of kinetic parameters was done using a plug-flow model. The K_M value observed for the immobilized enzyme was $1.9 \mu\text{M}$ which is similar to published values for horseradish peroxidase. Mass transfer effects were noted as important in low flowrate experiments but decreased in higher flowrate experiments. The same method of immobilization was used to create sequential reactions involving invertase, glucose oxidase, and horseradish peroxidase in the same device. The direction of flow and order of enzyme immobilization was studied. The reaction was shown to yield significant amounts of product only when the enzymes were placed in the correct order for the sequential reaction.

CHAPTER 3

EXPERIMENTAL

3.1 Materials

Hydrogen peroxide (30 wt%, Fisher Scientific), bovine liver catalase (C1345, Sigma Aldrich), 3-aminopropyltriethoxysilane (3-APTES, 99%, Acros Organics), glutaraldehyde (25 v/v%, Fisher Scientific), monobasic sodium phosphate (monohydrate, Fisher Scientific), dibasic sodium phosphate (heptahydrate, Fisher Scientific), cyclopentanone (99%, Sigma Aldrich), SU-8 2035 photoresist (Microchem Corp.), SU-8 Developer (Microchem Corp.), and polydimethylsiloxane (Sylgard 184 Elastomer, Dow Chemical) were used in this work. Polished silicon wafers were obtained from Montco Silicon.

3.2 Microdevice Fabrication

3.2.1 Silicon Master Mold

The schematic for the stamp fabrication process is shown in Figure 3-1. Polished 3.25 " silicon wafers were rinsed with acetone, isopropyl alcohol, and ethanol. After

drying, they were immersed in a sodium hydroxide bath. This decreased the contact angle at the silicon surface and allowed the photoresist to spread more evenly during the spin coating step. Wafers were thoroughly rinsed with deionized water and dried with pressurized air. Spin-coating (Chemat Technology, KW-4B) with SU-8 2035 photoresist was completed to form a uniform photoresist layer. Each wafer was then soft baked to evaporate the solvent and densify the photoresist film. This step was carried out minimizing ambient light to prevent any premature cross-linking. The desired photomask (CAD/Art Services) was fixed to the surface of each wafer using adhesive tape. A thick glass slide was placed over the photomask to ensure even surface contact between the mask and wafer. This assembly was exposed to ultraviolet light from a UV floodlamp (Uvitron Intelli-Ray 400). After UV exposure, a post-bake step was completed and each wafer was placed in a bath of SU-8 developer solution and gently agitated by hand to speed the removal of unexposed resist. For thicker layers, the wafer was selectively rinsed in certain areas (based on the design) with cyclopentanone prior to development. This was the same solvent that was baked off after spin coating and was used to decrease the viscosity of the unpolymerized photoresist. Wafers were rinsed with isopropyl alcohol and baked for several hours to strengthen the bond between the photoresist and the silicon surface. The Microchem data sheet for NANOTM SU-8 2000 products (Appendix A) was used to guide the parameter choices such as spin coating speed for the desired film thickness, baking temperatures, exposure times and so on. The optimum experimental conditions were established by conducting experiments.

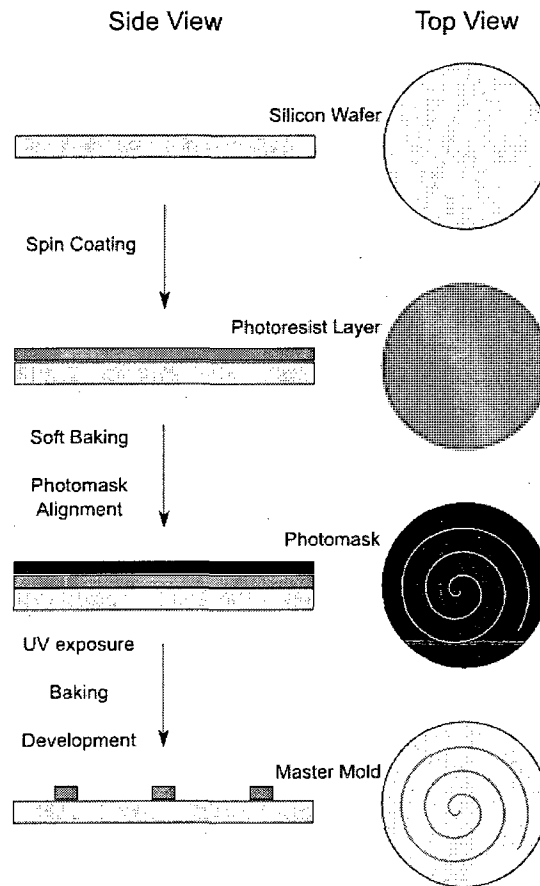


Figure 3-1: Schematic of the master mold fabrication process.

3.2.2 Inlet and Outlet ports

In order to access the channels for fluid flow, many procedures were used before a successful procedure was set. Cutting inlet and outlet ports was not successful in providing a sealed interface. Initially, PTFE tubing was used to directly interface with the device. This tubing was placed vertically on the silicon stamp such that it touched inlet and outlet locations on the photoresist. PDMS was poured and cured to create pre-formed ports. This method was modified to include pouring uncured PDMS into a cylindrical mold after inserting tubing in the pre-formed ports. A different modification using cyanoacrylate glue after initial pre-forming was attempted and was somewhat successful. This bond was inflexible, however, and did not remain

reliably sealed. The final procedure involved four steps. First, blunt tip needles (22 gauge, 1/2", Small Parts, Inc.) were placed vertically on inlet and outlet points on the master mold and secured in place using adhesive tape. Second, uncured PDMS was poured over the mold to cast a PDMS layer containing channel impressions with pre-formed inlet and outlet ports. Third, stainless steel hypodermic tubing (21 gauge, Small Parts, Inc.) was cut to short lengths and the ends were filed smooth and slightly rounded. This was accomplished by hand using an Arkansas stone to grind away any pinched or sharp edges. Finally, the needles were removed and the hypodermic tubing was carefully pushed into the pre-formed ports. The slight compression of the PDMS, caused by using hypodermic tubing of slightly larger diameter than the pre-formed holes, created a strong seal to interface the microscale device with macroscale tubing and equipment.

3.2.3 Casting and Sealing

The completed stamp with the inlet and outlet ports and a clean blank wafer were placed into standard size polystyrene petri dishes. The material used for the microdevices was polydimethylsiloxane (Sylgard 184, Dow Corning). It is relatively inexpensive, optically transparent, easy to work with, and forms irreversible bonds when exposed to oxygen plasma. Polydimethylsiloxane (PDMS) was created by mixing the prepolymer and curing agent in a 9 : 1 volume ratio and stirring. The stirring introduced many air bubbles into the viscous uncured mixture. These were removed by degassing in a vacuum chamber in order to create a homogeneous solid with smooth surfaces. The uncured degassed PDMS was then poured into the petri dishes containing the stamp and blank wafer. The dishes were placed into a 65°C

oven for 45 minutes to complete the curing phase. After curing completely, the petri dishes were removed, cooled, and the PDMS was carefully cut using a sharp precision knife. The cut PDMS was slowly peeled off and cleaned using pressurized air.

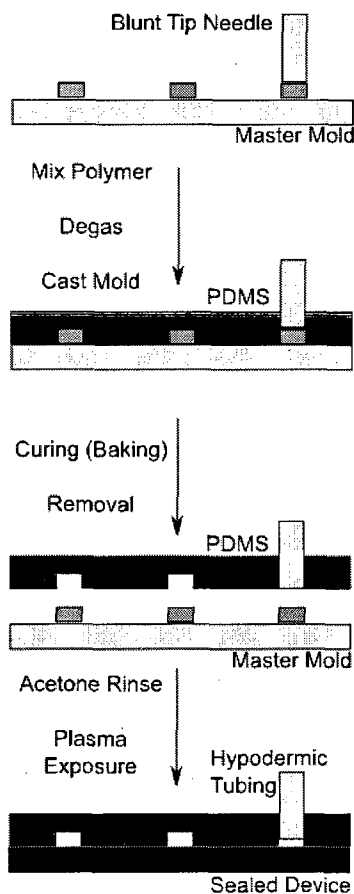


Figure 3-2: Casting and sealing procedure for microchannels.

Sealing provided many challenges to successful device fabrication and required significant time and effort to master. Incomplete seals caused many devices to fail with the reaction liquid leaking between the two layers. Ultimately a solution to this problem was reached and is presented here. The two layers were rinsed with acetone and placed on a glass slide with minimal surface contact. This was accomplished

by propping each layer up with a small scrap piece of PDMS and reduces the risk of sealing a layer to the glass slide itself. The slide was placed into a Plasma Cleaner (Harrick Plasma PDC-32G) and the chamber was placed under vacuum. It was flushed with pure oxygen and an RF generator was engaged to create the plasma. After 90 seconds of exposure the PDMS layers were removed and immediately placed in contact with each other. They were then placed in a 95°C oven under weighted glass slides for several hours to ensure a good seal. This baking step was crucial to having reliable seals. A success rate of approximately 33% was observed with less than one hour of baking. This increased to approximately 75% for 2 – 3 hours of baking time.

3.2.4 Interfacing

Interfacing the microscale device with macroscale equipment was accomplished by the following procedure as illustrated in Figure 3-3. For devices with flow channels, the inlet and outlet ports were formed by casting directly in the PDMS layer at curing time as described in Section 3.2.2. After peeling the PDMS layer off of the stamp, the needles were carefully pushed through the PDMS layer to ensure a smooth opening and then removed. Sealing took place as described in Section 3.2.3. Syringe pumps were used to drive fluid flow.

To connect the syringe pumps, the syringe was fitted with a 21 gauge blunt tip needle and a section of 22 gauge PTFE tubing of the desired length. Small sections of 21 gauge stainless steel hypodermic tubing were cut and prepared with an Arkansas stone. This involved grinding down any metal blocking the opening after cutting

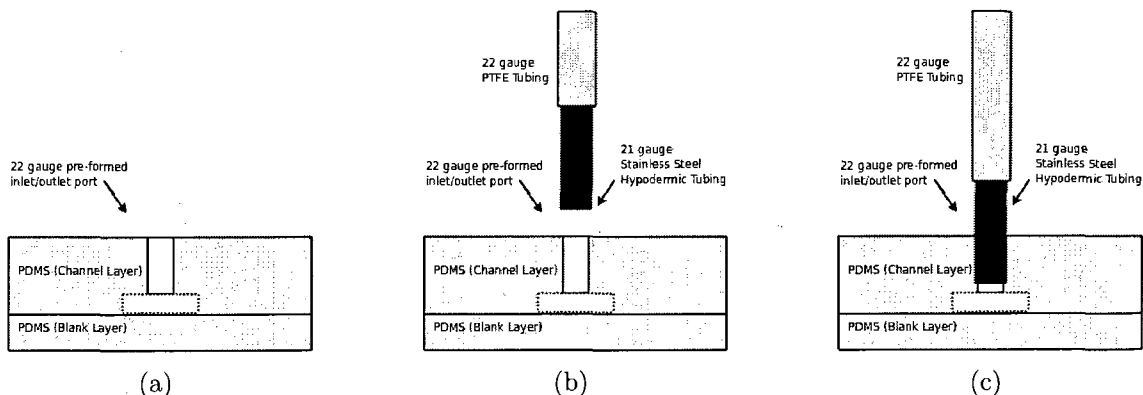


Figure 3-3: Procedure for interfacing the microchannels with macroscale equipment.

and slightly rounding the 90° corner on each cylinder edge. The edges of the needle attached to the syringe were also rounded off by the same method. The hypodermic tubing and needle were cleared of any debris using a 26 gauge needle. The hypodermic tubing was inserted into the PTFE tubing and into the desired pre-formed inlet and outlet ports on the microdevice. Rounding the edges slightly prevented the PDMS from being cut when inserting the stainless steel tubing. The tubing was slightly larger than the pre-formed inlet and outlet ports and the compression from the elastomeric nature of PDMS formed a conformal seal on the smooth stainless steel surface. This prevented leaks at the interface for the channels used in this work.

3.2.5 Reactor Designs

The microchannel reactors used in this work are shown in Figure 3-4. The different reactor designs provided varying volumes of reactor and geometries with different mixing properties. The three patterns also had different inlet configurations. For pattern A, the substrate and enzyme solutions entered the reactor at a T-junction with side entry. The pattern B had the substrate and enzyme solutions entering at a

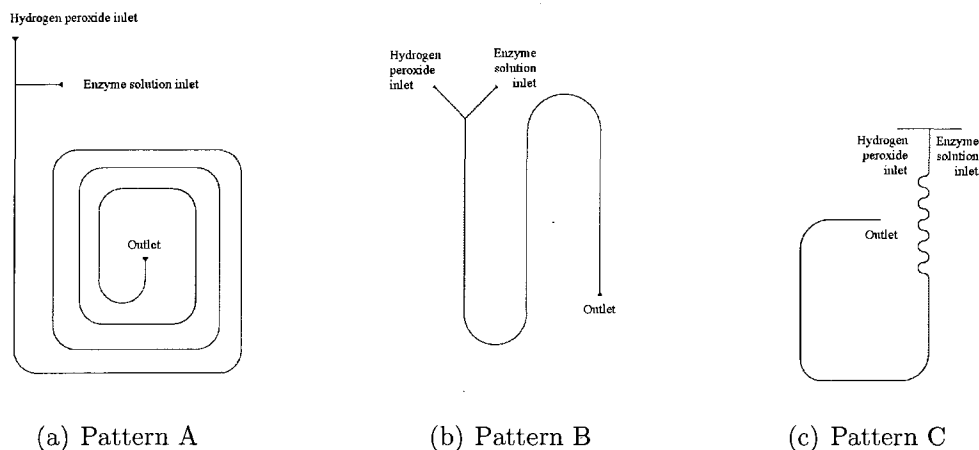


Figure 3-4: Channel designs used in the enzymatic reaction experiments.

Y-junction. In pattern C, the substrate and enzyme solutions entered at a T-junction with a head-on entry. The final dimensions of the fabricated channels for each design are listed in Table 3.1.

Table 3.1: Average device dimensions for designs listed in Figure 3-4. Error indicates largest variation between average and measured values.

Pattern	Width (μm)	Height (μm)	Length (μm)	Volume (μL)
A	304 ± 25	140 ± 22	322,923	14.2
B	126 ± 11	46 ± 4	123,252	0.7
C	164 ± 23	145 ± 11	172,523	4.1

3.3 Enzymatic Reactions in Microdevices

These devices were supported by a clamp attached to a stand and arranged such that fluid flow was parallel to the benchtop. Syringes were connected to the PTFE tubing and pressure driven fluid flow was controlled using syringe pumps. This setup was used for all non-particulate experiments. For experiments with carrier-free enzyme aggregates, a glass gastight syringe was loaded with a small stainless

steel ball bearing, which was slightly smaller in diameter than the inside diameter of the syringe. A filtered solution ($< 30\mu\text{m}$) containing aggregate particles was loaded into a glass gastight syringe containing the ball bearing and remaining air was cleared. The experimental apparatus used in the previous experiments was placed on a large flat board, which was then placed on a linear-oscillating shaking plate incubator. This equipment included two syringe pumps and a stand with clamps holding the microchannel device and collection platform. A second stand was set up near this equipment and used to hold a magnet stationary just above the body of the enzyme-containing syringe. This magnet held the ball bearing stationary relative to the benchtop. When the incubator was turned on, the syringe body followed the slow oscillatory pattern of movement and the entire experiment moved in unison. This motion of the syringe around the ball bearing provided steady mixing of the particulate solution and addressed the issue of particle settling which would have affected the enzyme concentration as additional particles settled over the course of the experiment. The experimental setup is shown in Figure 3-5.

The fluid exited the device and was collected in dropwise fashion. Static electricity buildup was observed repeatedly as the drops detached from the device outlet tubing and traveled diagonally downward and toward the wall of the glass collection vial. These drops were small enough that they did not slide down the wall until multiple drops had built up. By attaching to the wall, these drops took much longer to contact the quenching fluid, changing the effective residence time for the reaction. The experimental apparatus was subsequently grounded and static electricity buildup was dissipated each time a collection vial was set in place. This corrected the observed problem of drops flying to the sidewalls rather than falling directly into the fluid.

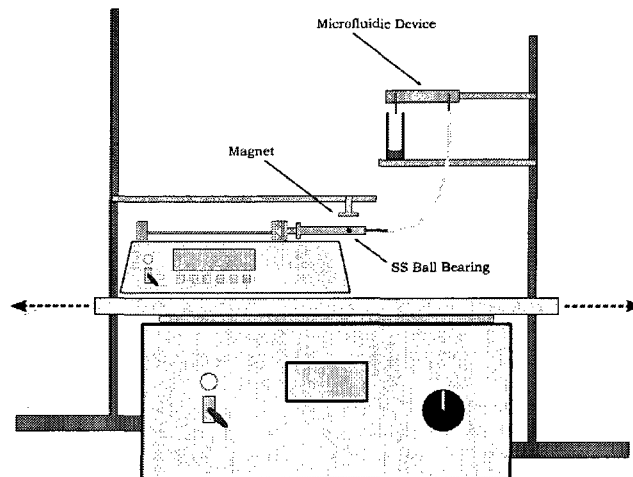


Figure 3-5: Schematic of the experimental apparatus for the carrier-free enzyme aggregate reactions.

3.3.1 Free Catalase Reaction

Initial experiments were conducted with free catalase in solution. Solutions containing catalase and hydrogen peroxide were flowed into the device and brought into contact at a channel intersection. The reaction mixture flowed through the device and reached an outlet well. Initial devices used fluid inlet and outlet wells as a design feature. For these experiments, an acidic fluid stream ($\text{pH} \sim 2.9$) was introduced into the outlet well to decrease the pH of the reaction mixture, deactivating the enzyme and quenching the reaction as it left the microchannel. Large variations were observed in the experimental data and the inlet and outlet wells were eliminated from the design. In order to quench the reaction, the reaction mixture exited the device and fell, in a dropwise fashion, into a collection vial containing a known volume of acidic quenching solution. This eliminated the large variations and allowed for the collection of reaction data.

Experiments were conducted using Pattern A. Two enzyme concentrations were

studied: ~ 12 U/mL and ~ 6 U/mL. The solution flow rates, concentrations, and the residence times for the experiments conducted are shown in Table 3.2. Initial substrate concentrations ranged from 0 to 100 mM.

Table 3.2: The experimental conditions used to conduct the free catalase reactions.

Case	Design	Enzyme Solution Flowrate	Substrate Solution Flowrate	Enzyme Solution Concentration	Residence Time (Drip Rate)
A1	A	4 μ L/min	4 μ L/min	~ 6 U/mL	120 s
A2	A	4 μ L/min	4 μ L/min	~ 12 U/mL	120 s

3.3.2 Enzyme Immobilization on Microdevice Wall

Microdevices were created and treated using several different reaction conditions. PDMS naturally presents a hydrophobic surface terminating in methyl groups. During plasma treatment, these groups are replaced by hydroxyl groups. Silanization followed by glutaraldehyde treatment has been shown to covalently bind enzymes to glass which has terminating hydroxyl groups at its surface. Several experiments were conducted using plasma treatment as the method of surface oxidation. Plasma treatment as a surface oxidation step limited the baking time available to strengthen the seal after exposure. Forty-five to sixty minutes was allowed for baking in these cases and the successful rate of sealing was approximately 33%. For successful devices, treatment then consisted of flowing a solution of 2.5 v/v% or 10 v/v % 3-aminopropyltriethoxysilane (3-APTES) in acetone, ethanol, or DI water through the microchannels followed by a rinsing step using the same solvent. Acetone based 3-APTES treatment presented the challenge of controlling evaporation within the

device. PDMS is permeable to gases and the acetone evaporated in nearly all cases before reaching the device outlet. The evaporation of the acetone solvent caused blockage of the channel due to the viscosity of the remaining solution in most cases. The use of acetone as a solvent for this step was determined to be an impractical method of treatment.

Ethanol was substituted for acetone which solved the problem of evaporation and was attempted at concentrations of 2.5 v/v % or 5 v/v % for 2 hours and 1 hour, respectively. This did allow the silanization step to complete without clogging the microchannels. The 3-APTES treatment was followed by glutaraldehyde at concentrations of 1 v/v % or 2 v/v % for 2 hours. Enzyme solution in concentrations of 10,000 U/mL or 50,000 U/mL was flowed through the device for several different time steps as small as 2 hours and as long as overnight.

The use of DI water as a solvent for the 3-APTES was attempted at concentrations of 5 v/v % and 10 v/v %. Glutaraldehyde treatment at a concentration of 5 v/v % followed. This method showed enzyme leaching.

A second method of oxidation [39] was used in an attempt to reduce the failure rate of devices and provide a more consistently oxidized surface. The sealing took place as normal and the post-plasma baking was used for several hours. The devices did show a much lower failure rate of less than 25%. After sealing, a solution of DI water, hydrochloric acid, and 30 wt% hydrogen peroxide (5 : 2 : 2 volume ratio) was flowed through the device and rinsed with DI water. Silanization with neat 3-APTES and glutaraldehyde treatment followed.

Patterns A and B were fabricated and catalase was immobilized on the channel

walls using the procedure described in Section 3.3.2. The 3-APTES, glutaraldehyde, and enzyme treatments were varied by changing the concentration, C, the flowrate, F, and the time for reaction, T, for 3-APTES, glutaraldehyde, and enzyme treatments. The different devices and treatment conditions are shown in Table 3.4. After the immobilization process was completed, substrate solutions were flowed through the device at 5 $\mu\text{L}/\text{min}$ for 40 minutes for Pattern A and 10 $\mu\text{L}/\text{min}$ for 20 minutes for Pattern B (see 3.3 for details). Combined with the 100 μL of quenching solution in the collection vial, a total of 200 μL was collected. This was the minimum sample size based on the available measuring equipment. Each change of substrate solution was preceded by a 20 minute deionized water rinse at the same flowrate.

Table 3.3: Experimental conditions used for experiments with immobilization of enzyme to the microdevice wall.

Case	Pattern	Substrate Solution Flowrate	Residence Time
A3	A	5 $\mu\text{L}/\text{min}$	2.8 min
A4	A	5 $\mu\text{L}/\text{min}$	2.8 min
B1	B	10 $\mu\text{L}/\text{min}$	0.07 min
B2	B	10 $\mu\text{L}/\text{min}$	0.07 min
B3	B	10 $\mu\text{L}/\text{min}$	0.07 min

3.3.3 Carrier-free Enzyme Aggregate Reaction

Cross-linked enzyme aggregates of catalase were created using the following procedure. Di(2-methoxyethyl) ether (diglyme), was chilled in an ice bath and a 125,000 U/mL catalase solution was added to achieve a 9:1 volume ratio of diglyme to enzyme solution. The enzyme was allowed to precipitate for 10 minutes and the reaction chamber (a glass vial) was removed from the ice bath. A magnetic stir bar was used

Table 3.4: Device and treatment conditions used for experiments with immobilization of enzyme to the microdevice wall. Concentration (C) is in v/v% for 3-APTES and Glutaraldehyde and in U/mL for the enzyme treatment. Flowrate (F) has units of $\mu\text{L}/\text{min}$ and time (T) has units of hours.

Case	Surface Treatment	3-APTES Treatment				Glutaraldehyde Treatment			Enzyme Treatment		
		C	F	T	Solvent	C	F	T	C	F	T
A3	Plasma	2.5	5	2	DI H_2O	2	5	2	100	3	8
A4	Plasma	2.5	5	2	EtOH	2	5	3	100	3	4.5
B1	Plasma	50	4	2.5	DI H_2O	1	4	2	10,000	4	2
B2	Liquid	10	4	2.5	DI H_2O	1	4	2	10,000	4	2
B3	Plasma	10	4	2.5	DI H_2O	1	4	2	10,000	4	2

to mix the solution throughout the reaction process. Glutaraldehyde (25%) was added to achieve a final concentration of approximately 10 mM. The crosslinking reaction was allowed to proceed for 2 hours at room temperature. After 2 hours, the total reaction volume was doubled by adding 0.1 M pH 10.0 sodium carbonate buffer. 1 mg/mL of sodium borohydride was added and the reaction mixture was stirred for an additional 30 minutes. At this point, a trace amount of Triton X-100 surfactant solution was added. This allowed the pelleted aggregate particles to be resuspended without difficulty after centrifugation. The solution was placed in microcentrifuge tubes and spun at 8,000 RPM for 10 minutes to create a soft pellet. The supernatant was pipetted off and the pellet was rinsed 3 times with 100 mM pH 7.0 sodium phosphate buffer. 50 mM pH 7.0 sodium phosphate buffer was used to resuspend the aggregates and filtration was carried out using 30 micron nylon mesh (Small Parts, Inc). Based on the measured channel size, the filtrate was saved and used as the enzyme solution for the results shown. The same batch of enzyme aggregate product was used for all tests. Aggregates were just visible to the naked eye and were quite

visible under a microscope.

The effect of acetone or diglyme as a precipitant on the reaction rate was first studied in a batch reactor. A spectrophotometer at 240 nm was zeroed using a solution containing 50 μL of quenching acid, 50 μL of aggregate particle solution, and 200 μL of deionized water. Acetone batch experiments were completed by first adding 50 μL of aggregate particle solution to a glass vial. Next, a timer was started just as 200 μL of substrate solution was quickly added to the vial and mixed. After three minutes, the reaction was halted by adding 50 μL of quenching acid. Absorbance measurements of this reaction mixture gave final value readings. Initial value readings were taken by measuring the absorbance of a mixture containing 50 μL of aggregate particle solution, 50 μL of quenching acid, and 200 μL of the appropriate substrate solution. It is important to note that these three solutions were added together in that order, ensuring that the substrate could not be consumed by the enzyme prior to taking an absorbance reading. This procedure was modified for the diglyme batch experiments due to the high activity of these aggregates. In the case of diglyme aggregates, 10 μL of aggregate solution, 390 μL of substrate solution, and 200 μL of quenching acid were used. The same procedure was completed using a reaction time of 1 minute.

As mixing was a major concern in flow experiments with enzyme aggregates, Pattern C with a head-on intersection was used. Flow reactions were carried out with diglyme-precipitated aggregates due to the far greater activity observed in batch reactions. Prior to flowing aggregates, an oxidizing solution containing a 4 : 1 : 1 ratio of deionized water, hydrochloric acid, and hydrogen peroxide was flowed through

the device. The device was then thoroughly rinsed with a pH 7.0, 50 mM sodium phosphate buffer. This oxidation step prevented aggregates from adhering to the channel surface. The enzyme solution and a substrate solution flowed into the device from separate channels. These came into contact at a head-on intersection and flowed through the length of the device. At the device outlet, the reaction mixture formed droplets that fell at a steady rate. Each drop fell into an acidic quenching solution as described before and analysis was carried out in the same way. A range of initial substrate concentrations was used to produce an initial rate plot.

Table 3.5: Experimental conditions used for carrier-free enzyme aggregate reactions.

Case	Design	Precipitant	Aggregate Solution Flowrate	Substrate Solution Flowrate	Residence Time
C1	C	diglyme	0.25 $\mu\text{L}/\text{min}$	9.75 $\mu\text{L}/\text{min}$	120 s
C2	C	diglyme	1 $\mu\text{L}/\text{min}$	9 $\mu\text{L}/\text{min}$	120 s

3.4 Analysis Techniques

3.4.1 Measurement of Channel Dimensions

The dimensions of the channel were measured optically using microscopy and a known standard image. Several cross sections of each PDMS device were taken by cutting with a small precision work knife. These cross sections were placed on a glass microscope slide and imaged using a CCD camera. A USAF Resolution Test grid image taken at the same magnification was used to calibrate the device images. The height

and width of the channel was measured and the average of several measurements for each dimension was calculated. The length was estimated using the known design length from the original photomask. This volume was used with the set flowrate to determine residence time within the device for non-quenched experiments. This method was used to determine the residence time and thus, reaction time, for early experiments where in-device reaction quenching was attempted.

3.4.2 Sample Collection

A small glass vial was placed beneath the device outlet tubing to collect fluid for sampling. When free enzyme or enzyme aggregate particles were used the reaction would continue in the collection vial after leaving the device. This is undesirable for studying the reaction in the device itself. In these cases, the reaction vial was filled with a known volume of an acidic solution. This decrease in pH deactivated the enzyme, quenching the reaction. The steady drip rate allowed consistency between each drop, providing a steady residence time for each drop, and allowing for calculation of reaction rate based on the residence time measured from the drip rate. The drip rate was obtained by measuring the time per drop from formation to breakup for several drops. This data was averaged to give an approximate residence time and is shown below in Table 3.6.

3.4.3 Measurement

Samples were pipetted into a quartz cuvette and placed in a UV-Vis spectrophotometer (Spectronic Genesys 2) zeroed to DI water. The substrate, hydrogen peroxide,

Table 3.6: Dripping rate for the drops exiting the microdevice for carrier-free enzyme aggregate experiments.

Drop	Time (s)
0	0
1	74
2	73
3	74
4	75
5	78
6	74
7	76
8	75
9	75
Average	75

has an absorbance peak at 240 nm. Absorbance measurements were taken at 240 nm and converted to concentrations using a standard curve. This curve, shown in Figure 3-6, was created using dilutions of the hydrogen peroxide when it was first received at a certified initial concentration.

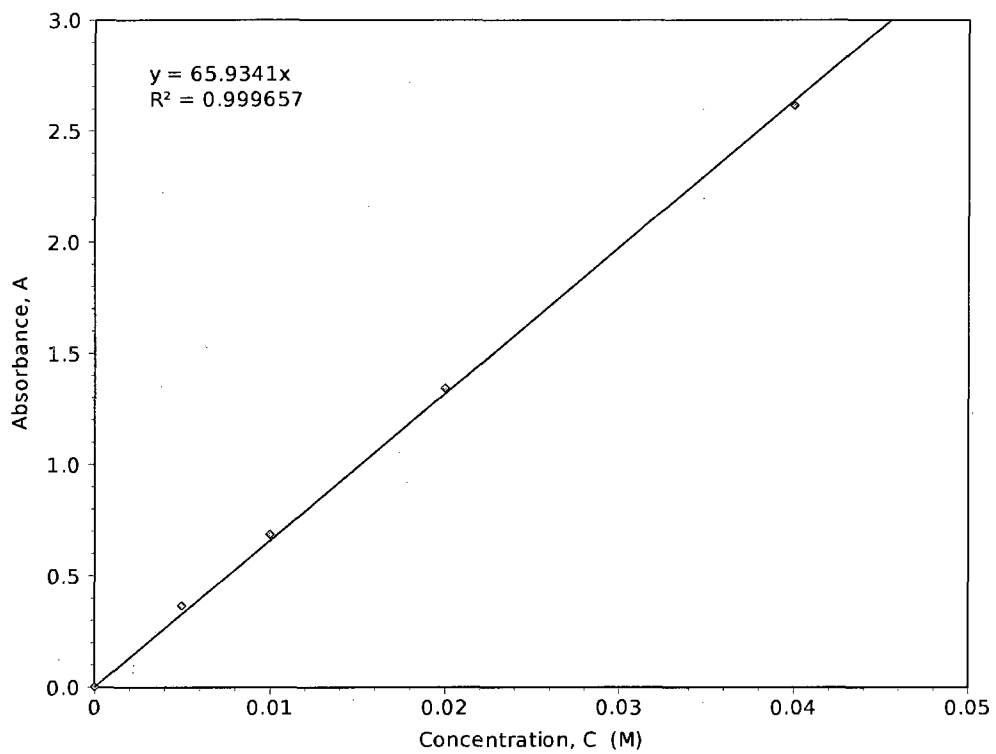


Figure 3-6: Standard calibration curve for hydrogen peroxide at a wavelength of 240 nm.

CHAPTER 4

RESULTS AND DISCUSSION

4.1 Microdevice Fabrication

Microdevices were fabricated by first creating a master mold of patterned photoresist on a polished silicon wafer and then using replica molding (REM) to create polydimethylsiloxane (PDMS) castings of the master mold. These PDMS castings were removed from the master mold and irreversibly sealed with a flat layer of PDMS to create devices containing microchannels for fluid flow. Using the Microchem data sheet for NANOTM SU-8 2000 products (Appendix A) as a guide, experiments were conducted to establish the optimal conditions for microdevice fabrication using soft lithography. The channel height corresponded to the thickness of the photoresist layer on the master mold. This thickness was controlled by the speed and duration of the spin coating step. Devices were fabricated with channel heights ranging from approximately 45 to 140 μm . Channel width was dependent on a combination of several fabrication steps. The design width of the channel on the photomask and the duration and temperature of the post-exposure baking step appeared to directly impact the channel width. Overbaking caused incomplete development such that

Table 4.1: Effect of changing certain process parameters on the silicon master mold fabricated.

Parameter	Effect
Low resolution photomask	Channel walls are not sharp
Shorter time for developing	White film formation Channel size larger
Longer time for developing	Entire photoresist layer detaches
No agitation of developer fluid	White film formation
Shorter UV exposure time	Channels are not sharp
Longer UV exposure time	Wider channels
No rotation of wafer during exposure	Wider channels

unexposed resist did not completely dissolve. This left undesirable residue on the master mold and resulted in misshapen walls. Increasing the length of the development step in these cases caused detachment of the cross-linked pattern from the silicon surface and thus prevented successful use of the resulting mold. Underbaking yielded finer design features, but frequently caused detachment of the cross-linked pattern at very short development times, again preventing the successful use of the resulting mold. The qualitative effect of changing certain fabrication process parameters on the master mold based on experimental observations are listed in Table 4.1. Quantitative effect of photomask resolution and rotation under a UV lamp are described in Sections 4.1.1 and 4.1.2. Based on these qualitative and quantitative data, the optimal procedure for master mold fabrication was established and is described in Section 4.1.3.

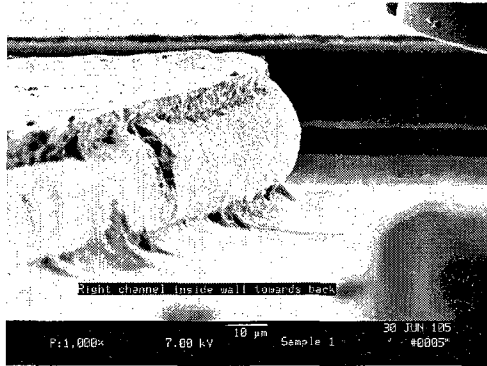
4.1.1 Effect of Photomask Resolution

The resolution of the photomask played a significant role in the quality of the channels created. Photomasks were ordered with a resolution equivalent to 5,000 dpi and

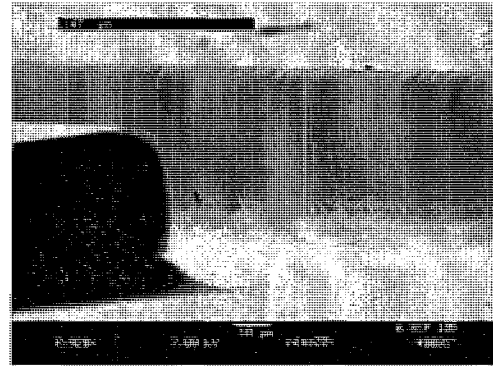
20,000 dpi. Differences between PDMS layers cast from master molds produced using low and high resolution photomasks are shown in Figure 4-1. These images were taken using a scanning electron microscope (Amray 3300 FE). Images (a), (b), and (c) correspond to a 5,000 dpi photomask and images (d), (e), and (f) correspond to a 20,000 dpi photomask. A clear difference in the smoothness and angle of the sidewalls is apparent. Images corresponding to the higher resolution photomask show a more uniform PDMS channel wall and sidewalls which are much closer to vertical. 20,000 dpi photomasks was determined to yield more desirable results than 5,000 dpi photomasks. Cross-sectional images of three sealed microchannel sections created from a master mold fabricated using a 20,000 dpi photomask are shown in Figure 4-2. Some variation does exist in the angle of sidewalls and imperfections in the generally rectangular shape are observed. The sealed channels have relatively uniform and vertical sidewalls and are representative of the results obtained from molds made using 20,000 dpi photomasks.

4.1.2 Effect of Rotation Under UV Lamp

Two master molds were fabricated using the same photomask of $100\mu\text{m}$ dimension and the same fabrication procedure with one major difference. In the fabrication of the first master mold, the coated silicon wafer was exposed to the UV lamp for 60 seconds in four 15 second intervals without rotating the wafer. In the fabrication of the second master mold, the coated silicon wafer was exposed to the UV lamp for 60 seconds in four 15 second intervals with 90° rotation of the wafer after each interval. PDMS microchannels were fabricated using these master molds and then sliced at different locations to measure the width of the microchannel. The variation of the



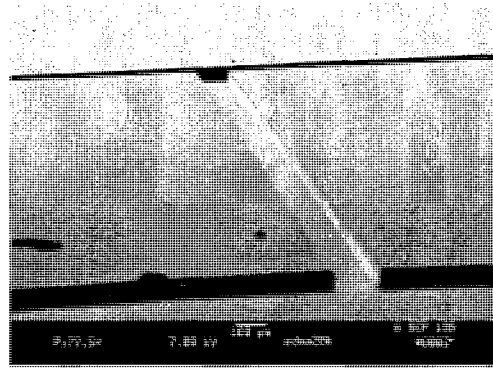
(a)



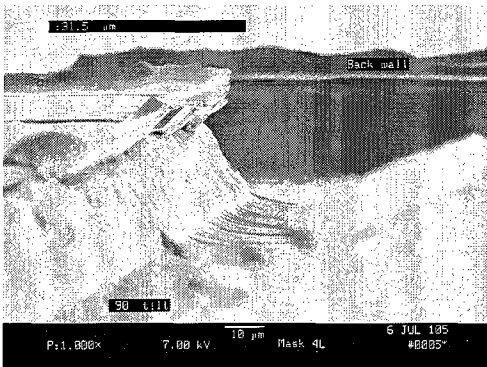
(d)



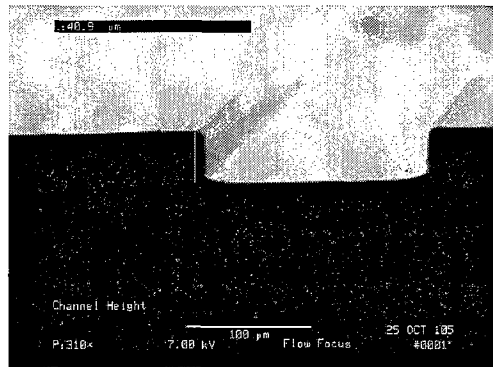
(b)



(e)

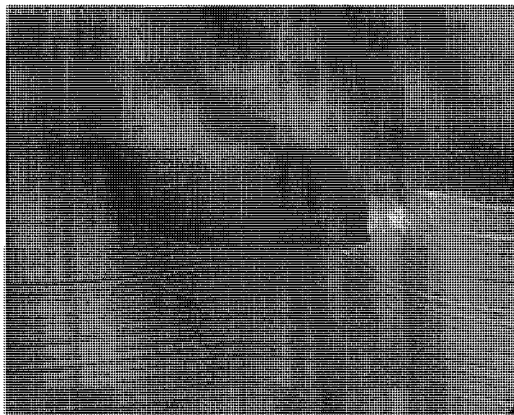


(c)

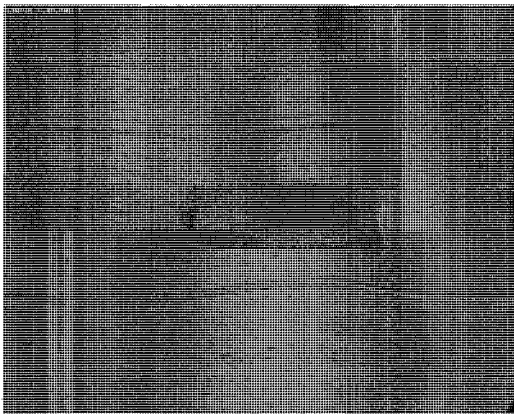


(f)

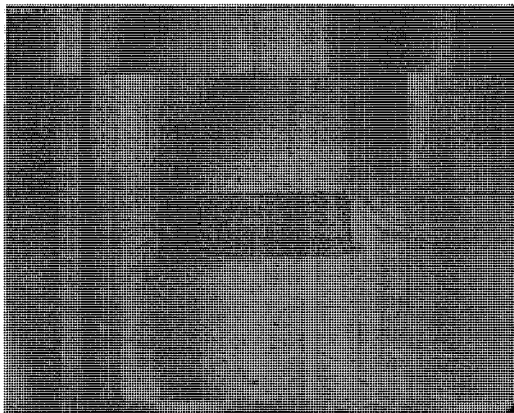
Figure 4-1: SEM images of PDMS layers cast from a stamp that was made using a (a)-(c) 5,000 dpi resolution photomask, and a (d)-(f) 20,000 dpi resolution photomask.



(a)



(b)



(c)

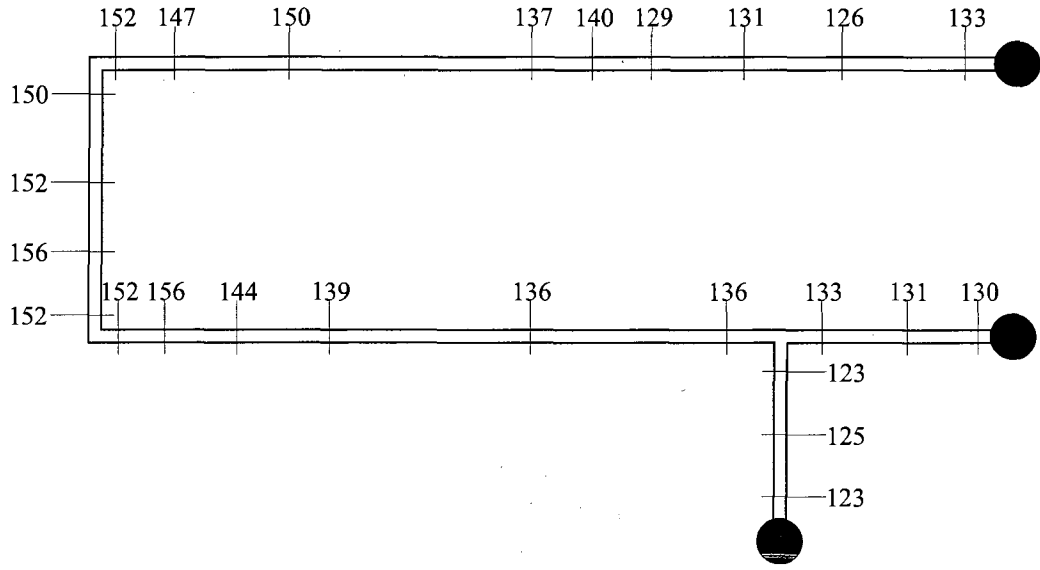
Figure 4-2: Cross-sectional images from three locations on a PDMS microdevice cast from a mold made using a 20,000 dpi photomask.

width of the microchannel along the microchannel for the two microchannels is shown in Figure 4-3. The microchannels in general have a higher width as compared to the design width of $100\mu m$. In the absence of rotation between the exposure intervals, the fabricated width was larger than in the presence of rotation between the exposure intervals. The wider fabricated widths of the channel as compared to the design widths and in the absence of rotation may be because the UV light source was not very collimated or the contact between the photoresist layer and the photomask was not very good.

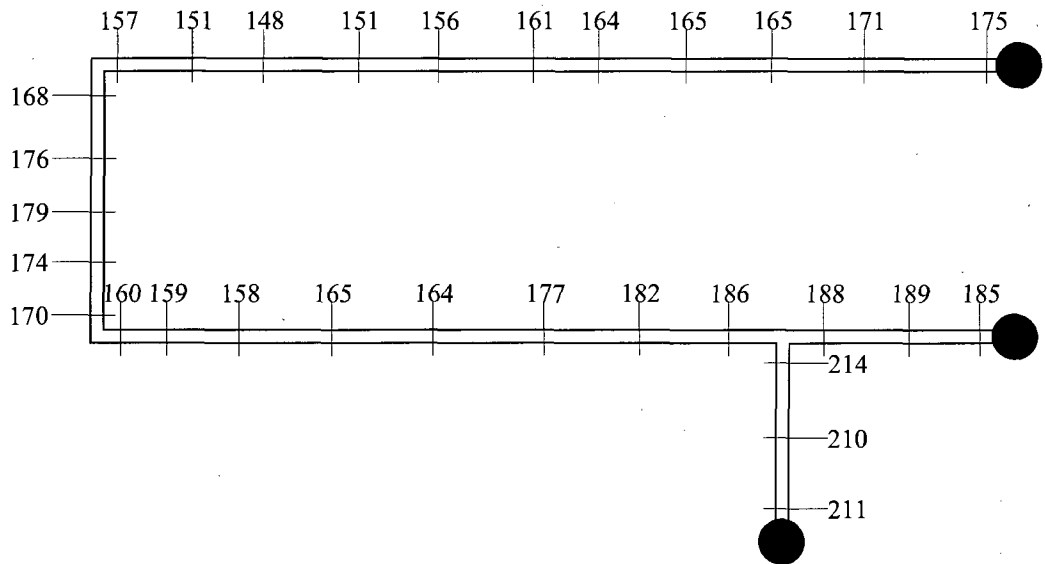
4.1.3 Master Mold Fabrication Procedure

Based on the experiments, the fabrication procedure that was used in creating the channels for this thesis is as follows:

1. The silicon wafer was washed with acetone, isopropyl alcohol, and ethanol to insure cleanliness.
2. The wafer was dried by baking at $65^{\circ}C$ for about 5 minutes.
3. The wafer was placed in a Petri dish containing 40% NaOH solution for approximately 10 minutes.
4. The wafer was rinsed with DI water and then baked again at $65^{\circ}C$ until completely dry.
5. The wafer was then placed on the spin coater and held in place using a 2" vacuum chuck. A puddle of approximately 3 mL of SU-8 2035 negative photo resist was poured on the wafer by running the resist down a slope to reduce



(a) exposed to UV light with rotation



(b) exposed to UV light without rotation

Figure 4-3: Dimensions in μm along the length of the microfluidic channel fabricated (a) with and (b) without rotation under the UV lamp.

the amount of bubbles in the resist. The amount of photoresist used was not particularly important as the spinning created an even coating.

6. The channel depth was altered by changing the speed used in the spin coater. For example, for a desired channel depth of $50\ \mu m$ the spin coater was run at a slow speed of 500 RPM for 7 seconds and a fast speed of 2000 RPM for 30 seconds.
7. The coated wafer was removed from the spin coater and baked at $95^{\circ}C$ for 45 minutes. After being removed from the oven the photoresist layer was dry.
8. A photomask of the channel design was placed over the wafer and then a large glass slide was placed on top to ensure good contact.
9. The wafer was placed 3" below the UV light source maintained at 100% intensity for a total of 60 seconds. Exposure was accomplished in 15 second intervals with a 90° rotation after each interval to ensure more even light exposure.
10. A post UV bake was then done for 3 minutes at $95^{\circ}C$.
11. After the post bake the wafer was placed in a Petri dish of SU-8 developer. The developer worked best when there was agitation, so constant swirling (by hand) was done for 10 minutes. After the agitation was done the wafer was put in a second bath of developer and left for 10 minutes. For thicker layers, the wafer was selectively rinsed in certain areas (based on the design) with cyclopentanone prior to development.
12. The wafer was rinsed with isopropyl alcohol and baked for several hours at $65^{\circ}C$ to strengthen the bond between the photoresist and the silicon surface.

Table 4.2: Dimensions in μm of the microfluidic channels fabricated from three master molds fabricated from the same photomask of $100\mu m$ width.

Mask No.	Width	Average Width	Height	Average Height
Mask 1	147 μm	151 μm	52 μm	53 μm
	161 μm		56 μm	
	144 μm		52 μm	
Mask 2	165 μm	163 μm	52 μm	55 μm
	162 μm		51 μm	
	163 μm		61 μm	
Mask 3	157 μm	161 μm	54 μm	55 μm
	180 μm		54 μm	
	146 μm		56 μm	

Three master molds were fabricated using the same 20,000 dpi photomask with a design channel width of $100\mu m$ to determine the variability in fabricating the microdevice channels. Three measurements of the channel height and width of the resulting device were made and are presented in Table 4.2. The difference between the designed and the fabricated dimensions depended on the pattern shape. A comparison of the photomask design features and resulting device dimensions for the three patterns used in this research is shown in Table 4.3. The most repeatable results obtained show a resulting channel width 1.5 – 3 times the size of the design feature on the photomask.

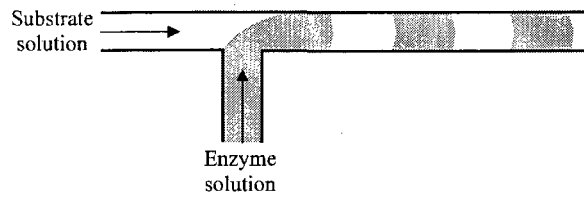
Table 4.3: Comparison of design and fabricated width for patterns used in this research. Average values are shown for fabricated width. Error indicates largest variation between average and measured values.

Pattern	Design Width	Fabricated Width
A	100 μm	304 \pm 25 μm
B	50 μm	126 \pm 11 μm
C	100 μm	164 \pm 23 μm

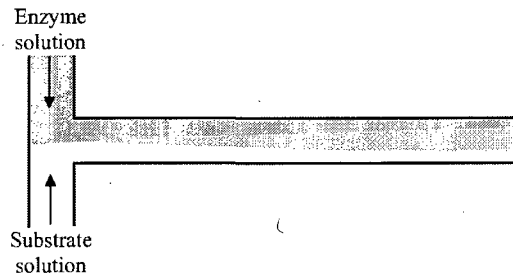
4.2 Enzymatic Reactions in Microdevices

Mixing within the microdevice is very important for the successful use of microdevices for enzymatic reactions. Some of the early enzymatic flow experiments in devices made from Pattern A showed an almost zero average rate of reaction. Since this pattern consisted of a T-junction with the enzyme solution entering as a side stream, it is possible that the flow was striated after the T-junction as shown in Figure 4-4(a). This resulted in the reaction taking place only at the interface between the slugs of the two solutions instead of the entire volume of the reactor and may explain the negligible rates of reaction. Better results were obtained at higher flow rates and higher enzyme concentrations. However, the existence of striated flow in the microchannel at higher velocities could not be ruled out. To alleviate some of these concerns, Pattern C was designed using a T-junction with a head-on entry. The expected flow pattern in this case is shown in Figure 4-4(b). To improve the mixing between the two solutions, a serpentine channel was introduced after the two solutions mixed as seen in Figure 3-4(c).

The free enzyme and the carrier-free enzyme aggregate reactions in this research could be visualized as a model reactor series scheme of a tubular flow reactor followed by a fed batch reactor as shown in Figure 4-5. The reaction mixture enters the tubular flow reactor at a flow rate Q with substrate concentration $[S]_0$ and the average exit substrate concentration is $[S]_1$. The reaction mixture then flows into a fed batch reactor and is emptied at time τ_{FB} . At this time, the average substrate concentration of the reaction mixture is $[S]_f$. Within the microchannel, mixing is only due to diffusion and gradients will exist along the channel cross-section. For simplicity, it is



(a) Slug flow pattern



(b) Parallel flow pattern

Figure 4-4: Flow patterns with (a) slug flow and (b) parallel flow possible in the microdevices.

assumed that the microchannel behaves as a plug flow reactor with a residence time τ_{PFR} . As the drop forms at the end of the microchannel, mixing is not controlled and gradients in substrate concentration may exist within the drop. Again for ease of analysis, the fluid in the drop is assumed to be well mixed. It is also assumed that when the drop falls, there is no fluid left in the fed batch reactor. Experimentally, τ_{PFR} and τ_{FB} are known from the channel design and set flow rate, Q , and the initial and final substrate concentrations, $[S]_0$ and $[S]_f$ are measured. The reaction with enzyme immobilization on the microdevice wall can be analyzed as just a plug flow reactor.

Assuming that Michaelis-Menten reaction kinetics describes the decomposition of

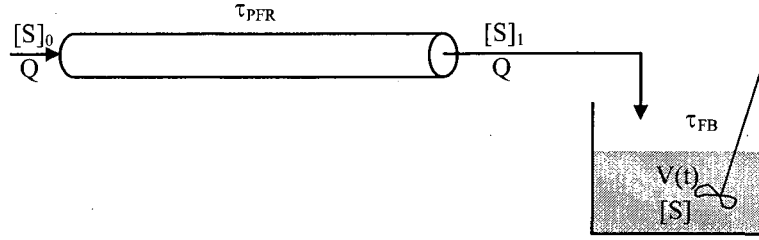


Figure 4-5: Model reactor series scheme to analyze the microdevices in this research.

hydrogen peroxide, the general mole balance can be written as

$$\frac{d[S]_{PFR}}{d\tau} = -\frac{v_{max}[S]_{PFR}}{K_M + [S]_{PFR}}. \quad (4.1)$$

Here $[S]_{PFR}$ is the substrate concentration at residence time τ in the plug flow reactor.

Integrating between the limits $[S]_{PFR}(\tau = 0) = [S]_0$ and $[S]_{PFR}(\tau) = [S]_{PFR}$ gives an implicit equation for calculating $[S]$ at any residence time τ as

$$K_M \ln \left[\frac{[S]_0}{[S]_{PFR}} \right] + [S]_0 - [S]_{PFR} = v_{max}\tau. \quad (4.2)$$

The substrate concentration at the exit of the plug flow reactor is calculated using $[S]_{PFR}(\tau = \tau_{PFR}) = [S]_1$. In the limit where $[S]_0 - [S]_{PFR} \ll [S]_0$, Equation 4.2 reduces to a linear relationship between substrate concentration and time,

$$\frac{[S]_0 - [S]_{PFR}}{[S]_0} = \frac{v_{max}}{K_M + [S]_0}\tau \quad (4.3)$$

The reaction mixture then enters the fed batch reactor at time $t = 0$ where the

general mole balance for the substrate can be written as

$$\frac{d[[S]V]}{dt} = Q[S]_1 - \frac{v_{max}[S]}{K_M + [S]}V. \quad (4.4)$$

The volume of the fed batch reactor at any time t is given by $V(t) = Qt$ assuming $V(t = 0) = 0$. Assuming Q to be constant and using the product rule, the substrate concentration in the reactor at any time, $[S]$ is given as

$$\frac{d[S]}{dt} = \frac{[S]_1 - [S]}{t} - \frac{v_{max}[S]}{K_M + [S]}. \quad (4.5)$$

This equation can be integrated numerically from $[S](t = 0) = [S]_1$ to $[S](t = \tau_{FB}) = [S]_f$ to determine the substrate concentration measured at the end of the microdevice. It should be noted that v_{max} is dependent on the amount of enzyme present in the reactor. In a fed batch reactor, v_{max} is not really a constant as the amount of enzyme increases continuously. In the present analysis, v_{max} is assumed to be a constant in the fed batch reactor.

The evolution of the substrate concentration as a function of residence time using Equations 4.1 and 4.5 is shown in Figure 4-6. For this data $[S]_0 = 30$ mmol/L, $v_{max} = 6$ mmol/L-min, $K_M = 35$ mmol/L, $\tau_{PFR} = 2$ min, and $\tau_{FB} = 1.25$ min. A nearly linear reduction in the substrate concentration with residence time is observed for both the plug flow reactor and the fed batch reactor. In the experiments, we set τ_{PFR} , τ_{FB} and measure $[S]_0$ and $[S]_f$. The results presented in the following sections will be recast as an average reaction rate, $[S]_0 - [S]_f/\tau_{TOT}$ versus $[S]_0$ where $\tau_{TOT} = \tau_{PFR} + \tau_{FB}$. The effect of v_{max} and K_M on the average reaction rate is shown

in Figures 4-7 and 4-8. The average reaction rate increases almost linearly with initial substrate concentration at low substrate concentrations. As v_{max} is increased, the average reaction rate increases as expected. A larger K_M value corresponds to mass transfer limitations and hence a reduced reaction rate as seen in Figure 4-8. Finally, for reactions with enzyme immobilization on the microdevice wall, Figure 4-9 shows the expected average reaction rate as a function of the initial substrate concentration for $v_{max} = 6$ mmol/L-min, $K_M = 35$ mmol/L, and $\tau_{PFR} = 2$ min. For comparison, the results for the series reactor scheme for $\tau_{FB} = 1.25$ min is also plotted on the same figure. The general trend of the average reaction rate versus the initial substrate concentration is the same as seen for the free enzyme and the carrier-free enzyme aggregate reactions. As expected, the average reaction rate is higher in the absence of a fed batch reactor.

4.2.1 Free Catalase Reaction

Initial experiments focused on demonstrating measurable reaction rates within a microdevice using free catalase and substrate solutions. This reaction began at the intersection of two channels and ended by quenching in acidic solution. The free catalase reactions were conducted in devices with Pattern A and a residence time of 120 seconds within the microchannel (i.e. $\tau_{PFR} = 2$ min) and a residence time in the drop of 75 seconds (i.e. $\tau_{FB} = 1.25$ min) before the reaction mixture was quenched. The average reaction rate, $[S]_0 - [S]_f / \tau_{TOT}$, versus the initial substrate concentration $[S]_0$ for the free enzyme reaction cases is shown in Figure 4-10. As initial substrate concentration increases, the average reaction rate increases almost linearly and reaches a maximum. After this maximum, substrate inhibition is observed and the

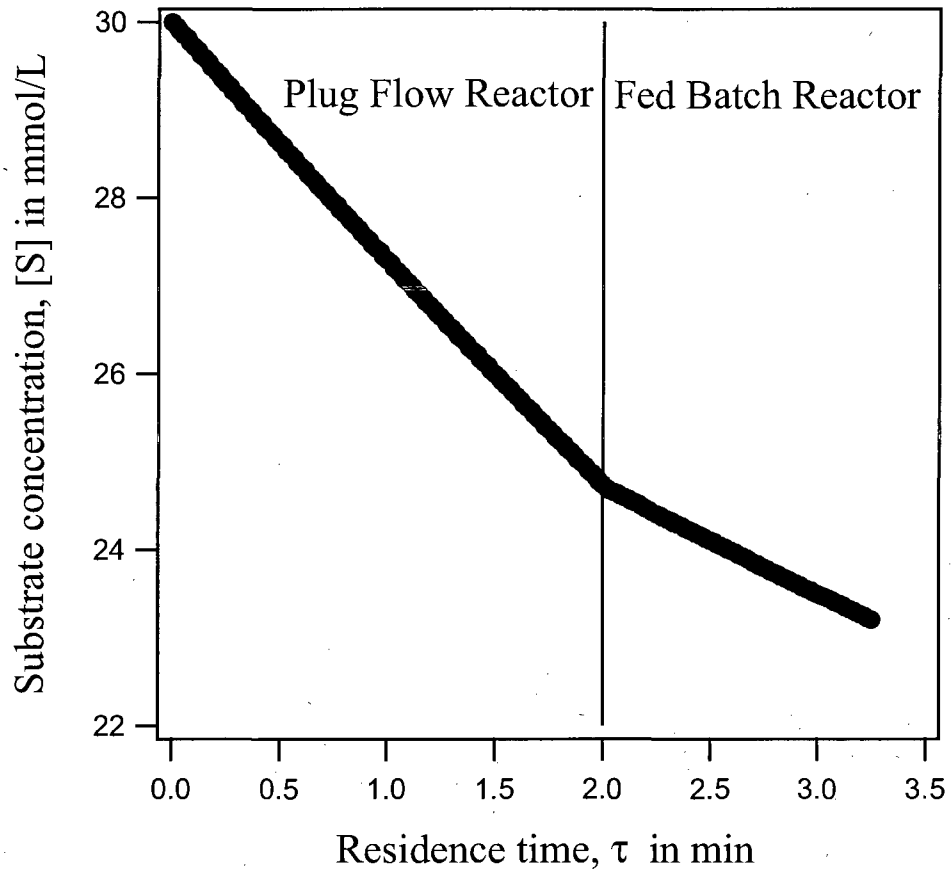


Figure 4-6: Evolution of substrate concentration with residence time for the model problem with $[S]_0 = 30$ mmol/L, $v_{max} = 6$ mmol/L-min, $K_M = 35$ mmol/L, $\tau_{PFR} = 2$ min, and $\tau_{FB} = 1.25$ min.

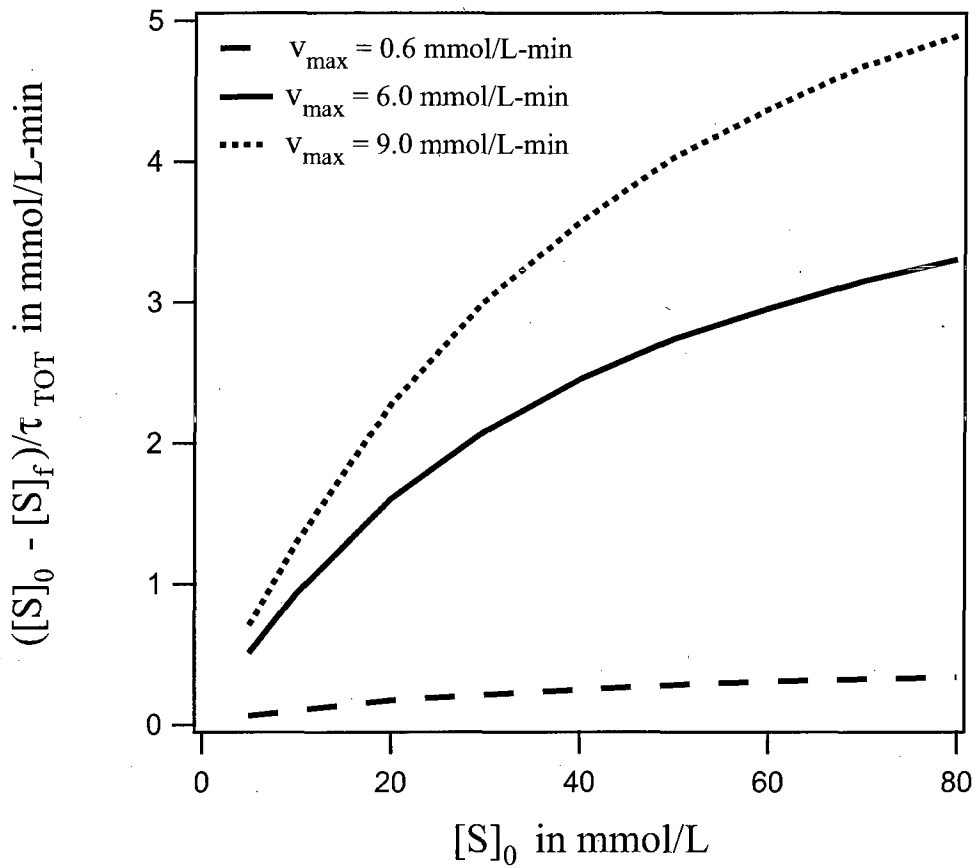


Figure 4-7: Effect of v_{max} on $[S]_0 - [S]_f/\tau_{TOT}$ as a function of initial substrate concentration $[S]_0$. $K_M = 35$ mmol/L, $\tau_{PFR} = 2$ min, and $\tau_{FB} = 1.25$ min.

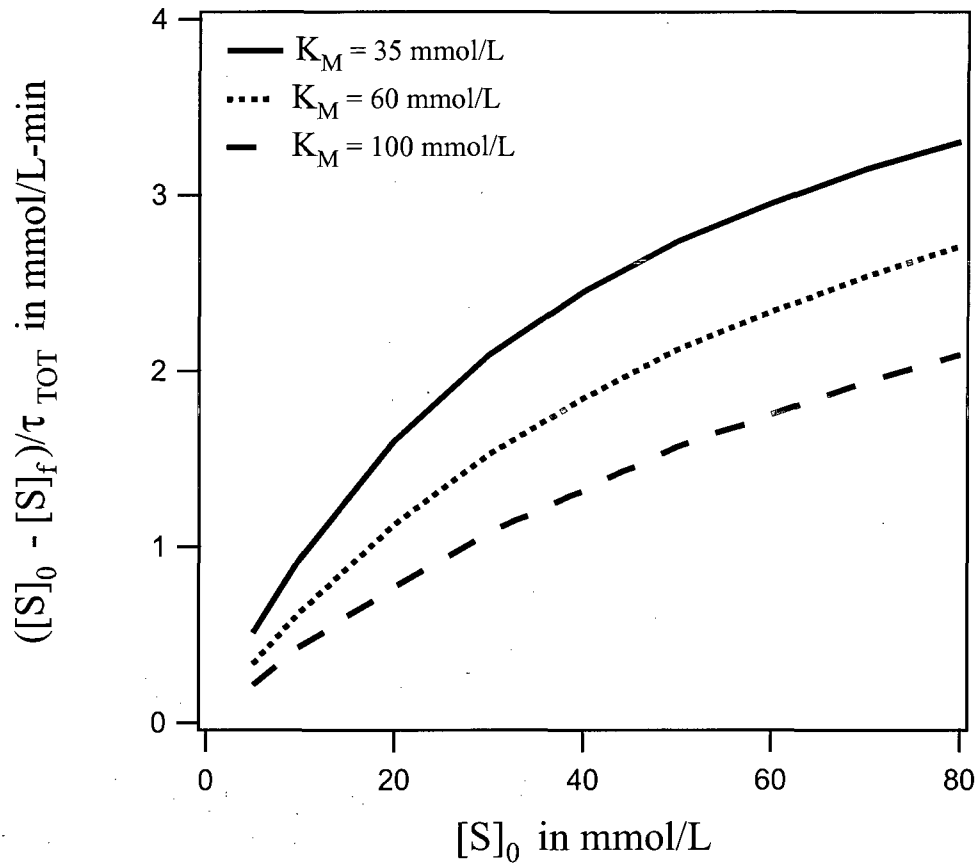


Figure 4-8: Effect of K_M on $[S]_0 - [S]_f/\tau_{TOT}$ as a function of initial substrate concentration $[S]_0$. $v_{max} = 6$ mmol/L-min, $\tau_{PFR} = 2$ min, and $\tau_{FB} = 1.25$ min.

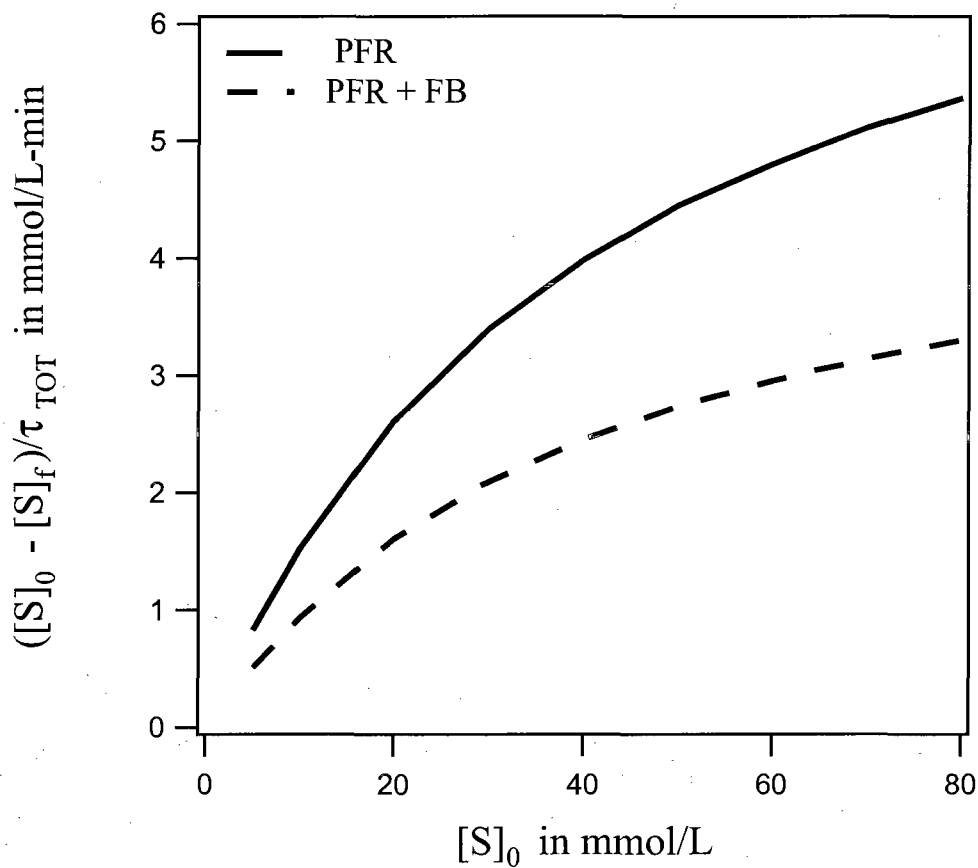


Figure 4-9: Average reaction rate as a function of initial substrate concentration in the absence and presence of a fed batch reactor with $v_{max} = 6$ mmol/L-min, $K_M = 35$ mmol/L, $\tau_{PFR} = 2$ min, and $\tau_{FB} = 1.25$ min.

average reaction rate decreases with further increase in the initial substrate concentration. In the macroscale experiments, this maximum is observed at ~ 80 mmol/L of initial substrate concentration which is consistent with the experimental data here. While the data does show a lot of scatter, the trend is consistent with the analysis results of Figure 4-7. However, without being able to measure the concentration at the end of the microchannel, it is not possible to calculate an exact v_{max} and K_M value.

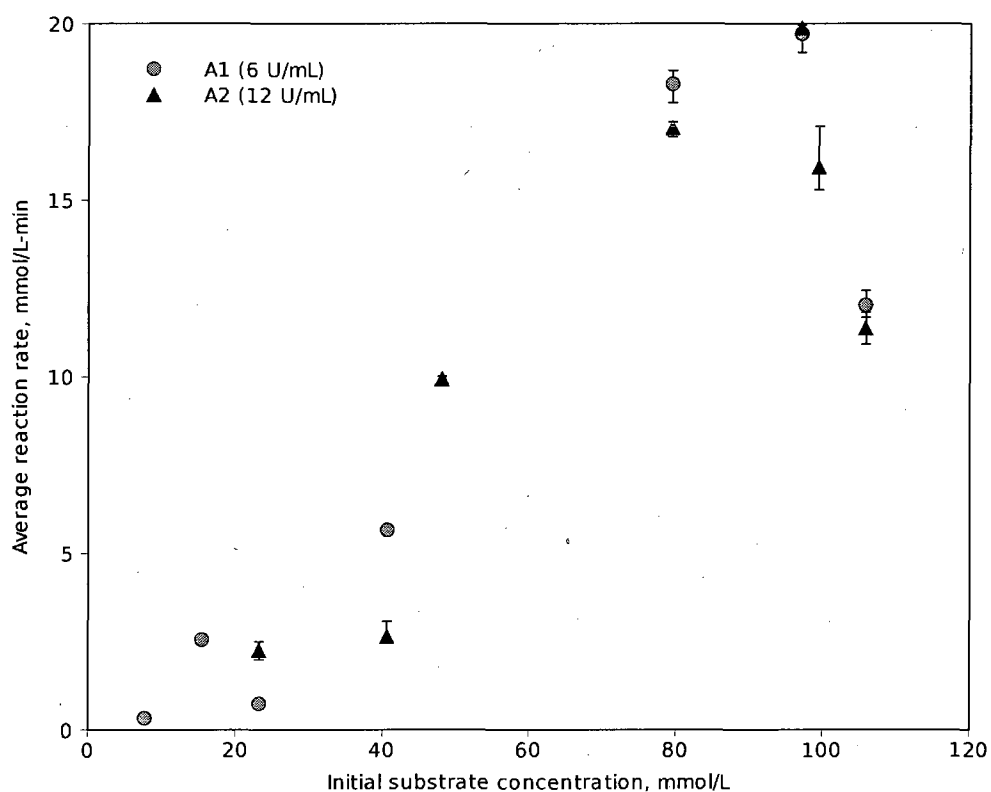


Figure 4-10: Initial reaction rate results for the decomposition of hydrogen peroxide by a solution of 6 U/mL and 12 U/mL of bovine liver catalase in a PDMS microdevice. Design features and reaction conditions correspond to experimental conditions A1 and A2 in Table 3.2.

4.2.2 Enzyme Immobilization on Microdevice Wall

For carrier-bound immobilization on microdevice wall, Patterns A and B were used with various treatment conditions. The average reaction rate as a function of the initial substrate concentration is shown in Figures 4-11 and 4-12. Results from the plasma oxidation method are shown in Figure 4-11 and results from the liquid phase oxidation method are shown in Figure 4-12. Furthermore, in Figure 4-12, the two data sets labeled B1 were collected starting with the lower initial substrate concentrations. In the data set labeled B2, data was collected starting with the higher initial substrate concentrations. For all variations on the silanization and binding procedure, the data shows a maximum in the reaction rate followed by a decrease in reaction rate as initial substrate concentration increases. However, this maximum does not occur consistently at the experimentally observed initial substrate concentration of 80 mmol/L. The observed data suggests that the enzyme did not irreversibly bind to the channel wall and was continuously leaching from the channel wall. The reaction rates observed followed the same general trend where initial data showed a high reaction rate that steadily dropped off at subsequent data points. This is consistent with detachment of the enzyme from the channel wall. As additional data points are collected, the total amount of enzyme in the system decreases, resulting in a consistent decrease in reaction rate despite the increased substrate concentration. Since the extent of leaching depended on the amount of time the channel was in service before the next measurement, the drop in the average reaction rate occurred at different initial substrate concentrations for the different runs. This is clearly seen in Figure 4-12 where the data showed a reduction in the average reaction rate depend-

ing on the order in which the data was collected immaterial of the initial substrate concentration.

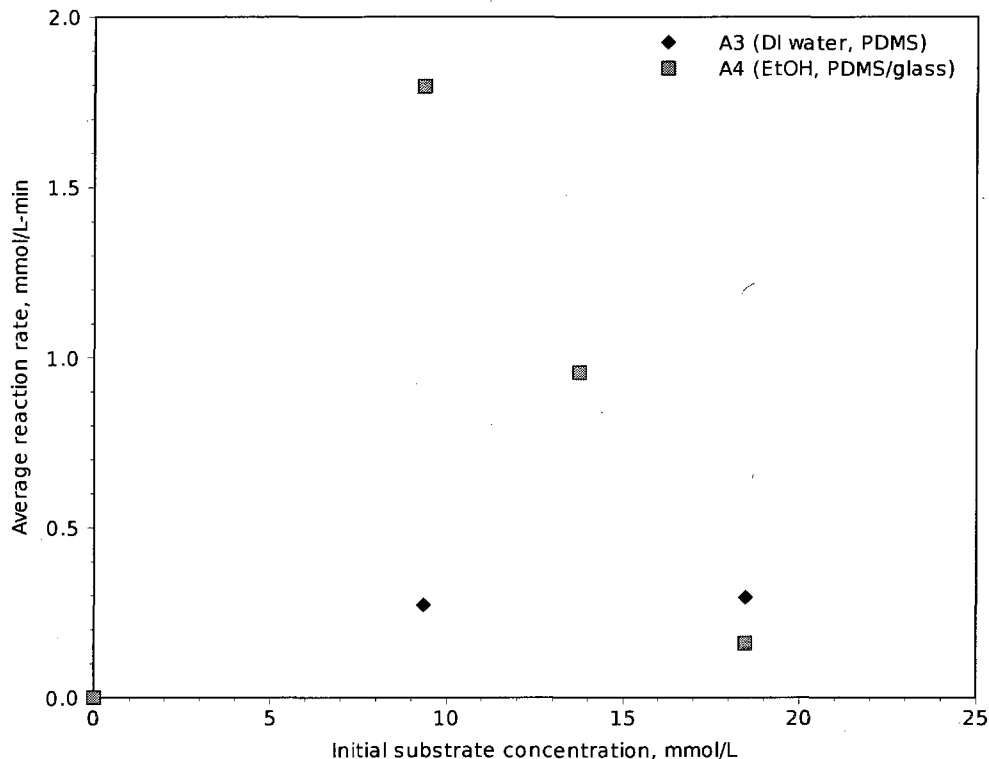


Figure 4-11: Average reaction rate versus initial substrate concentration for experiments with enzyme immobilization on microdevice walls for the conditions specified in Table 3.4.

Leaching was also confirmed by calculations examining the activity of the enzyme. At a starting concentration of 10 mmol/L, pH 7.0, and temperature of 20 °C, one unit of catalase decomposes one micromole of hydrogen peroxide over the course of one minute. Based on data collected for starting concentrations of approximately 10 mmol/L hydrogen peroxide, the change in absorbance over the actual residence time within the reactor results in a reaction rate that is impossibly large. This rate is significantly higher than what would physically be possible in an immobilized system. The observed rate exceeds the theoretical maximum rate possible based on the total mass of enzyme flowed through the device during treatment. Even if

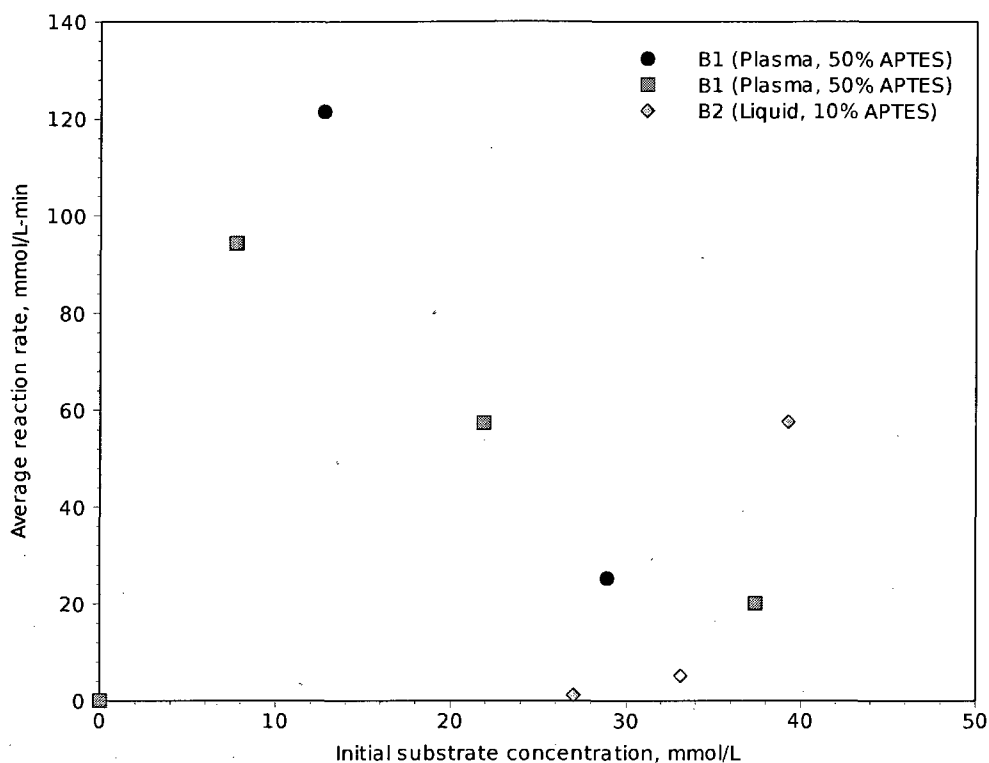


Figure 4-12: Average reaction rate versus initial substrate concentration for experiments with enzyme immobilization on microdevice walls for using the conditions specified in Table 3.4. Data points in both B1 series were taken starting at low initial substrate concentrations and progressing higher. In the B2 series, data collection started with a high initial substrate concentration and progressed to lower amounts.

the total mass of enzyme present in the device had bound to the channel walls and retained its native activity the reaction rate could not reach the measured value.

These calculations are presented in Table 4.5. Channel dimensions from Table 3.1 were used in these calculations. If the enzyme had leached from the channel walls,

Table 4.4: Parameters for calculation of total enzyme exposed to channel walls during treatment. Protein concentration provided by manufacturer.

Concentration U/mL	Flowrate uL/min	Treatment Time min	Protein Concentration U/mg protein	Total Enzyme mg protein
10,000	5	120	4540	0.661

the reaction would continue beyond the boundaries of the device including within the

sample collection vial. This effectively increases the residence time for the reaction beyond the calculated amount which explains the increased rate observed. Thus, it is concluded that enzyme leaching was taking place and the treatment methods were not successful in their goal of irreversibly binding the enzyme to the channel walls. Based

Table 4.5: Parameters used for calculation of observed activity and total enzyme present.

Initial Substrate Concentration	$\frac{\Delta \text{Concentration}}{\Delta \text{time}}$	Protein Concentration	Total Enzyme
9 mM	98136 U	4540 U/mg protein	21.6 mg protein

on the consistent results obtained for covalent bonding of catalase to PDMS using silanization followed by glutaraldehyde in cases of plasma and liquid phase oxidation, it was determined that these methods were not viable for irreversible binding.

4.2.3 Carrier-free Enzyme Aggregate Reaction

After confirming the results for covalent bonding methods, a new approach was taken. Immobilization of the enzyme as cross-linked enzyme aggregate particles was attempted and successfully achieved. An image of two aggregate particles prior to filtration is shown in Figure 4-13. It was determined that the choice of precipitant was imperative to retaining enzyme activity. Initial attempts at creating cross-linked catalase aggregate particles using acetone as a precipitant produced aggregates with nearly zero activity. Substitution of diglyme for acetone, as used by Guisán, Pessela et. al. [49], produced particles that retained a significantly higher level of activity. Batch reactions on these particles confirmed this retention of activity. An initial rate plot of the two batch reactions is shown in Figure 4-14. The diglyme data shown is



Figure 4-13: Image of two cross-linked catalase aggregate particles at 40x magnification. This image was taken prior to filtration.

the average of three trials. Error bars on these data indicate the high and low values and the data points represent the average value of the three sets. Acetone data are for one trial. The same preparation methods and filtration steps were used for each set of aggregates.

Michaelis-Menten kinetics are observed for the aggregates precipitated using diglyme. A Lineweaver-Burk plot of the diglyme batch data is shown in Figure 4-15. The slope and intercept of the linear regression yielded a K_M of 199 mmol/L and a v_{max} value of 630 mmol/L-min. An estimate of the total enzyme present was not made. Zheng et. al. [52] report a K_M value of 62 mmol/L for bovine liver catalase in solution which was used in microchannels. In their work, aqueous droplets were used as microreactors carried through the device by a bulk silicone oil. An increase in K_M as compared to the free enzyme K_M value is expected due to immobilization.

Initial experiments using these particles in microchannels showed aggregation of the particles near the channel entrance and some adhesion to the channel walls. Two

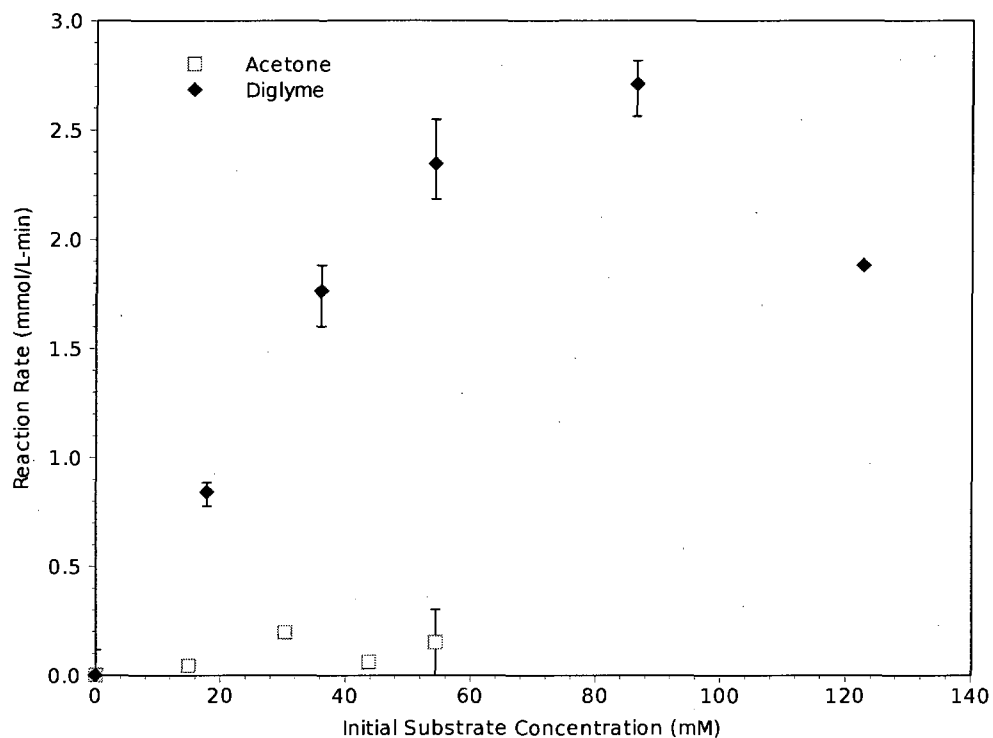


Figure 4-14: Initial reaction rate as a function of the initial substrate concentration for two batches with enzyme aggregates using diglyme and acetone as precipitants in the formation of the cross-linked enzyme aggregates.

steps were taken to alleviate this problem. Channels were treated with the same oxidizing solution used in covalent bonding experiments to make the walls temporarily less hydrophobic and more hydrophilic. A drop of Triton X-100 surfactant was added to the particle solution upon resuspension during their preparation. This appeared to solve the problem of aggregation and unpredictable flow of the enzyme particles through the device. Data were then collected for reactions involving a range of initial substrate concentrations. Results for aggregates made with diglyme and used in microchannel flow experiments are shown in Figure 4-16. Two volumetric flowrate ratios were used to test for activity in the microchannels. Initially, a ratio of 1:39 (enzyme to substrate) was used which resulted in very low activity. The data did not show the expected trend of increasing reaction rate with increasing initial substrate

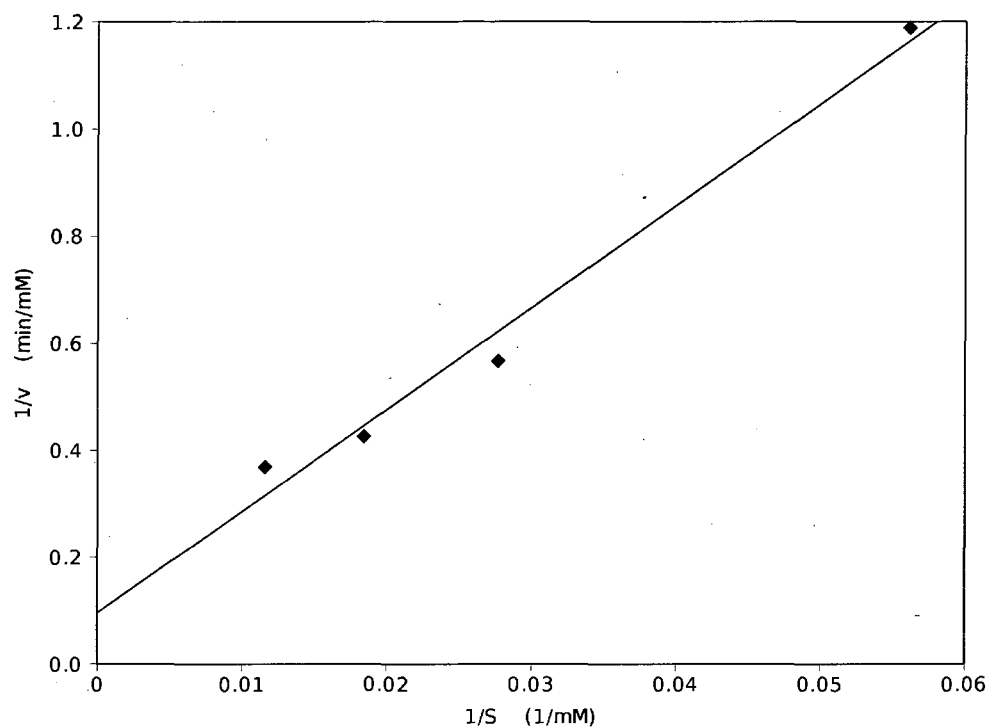


Figure 4-15: Lineweaver-Burk plot of batch reactions using diglyme precipitated aggregates.

concentration until a maximum was reached and the reaction rate would then drop likely due to substrate inhibition. The syringe pumps used in this research function by turning a threaded rod in discrete motions. To maintain a desired flowrate the frequency of these motions is determined based on the syringe diameter. Based on the syringes used, it was possible that not enough enzyme was present and distributed in the solution to show measurable activity. The ratio of enzyme solution to substrate solution was increased to 1:9 to provide more aggregate particles for reaction. This created a distinct difference in the results. The average reaction rate now showed a maximum at an initial substrate concentration of ~ 80 mmol/L which is consistent with the free enzyme reactions and the macroscopic batch reactions. As in the case of free enzyme reactions, a value for v_{max} and K_M could not be calculated.

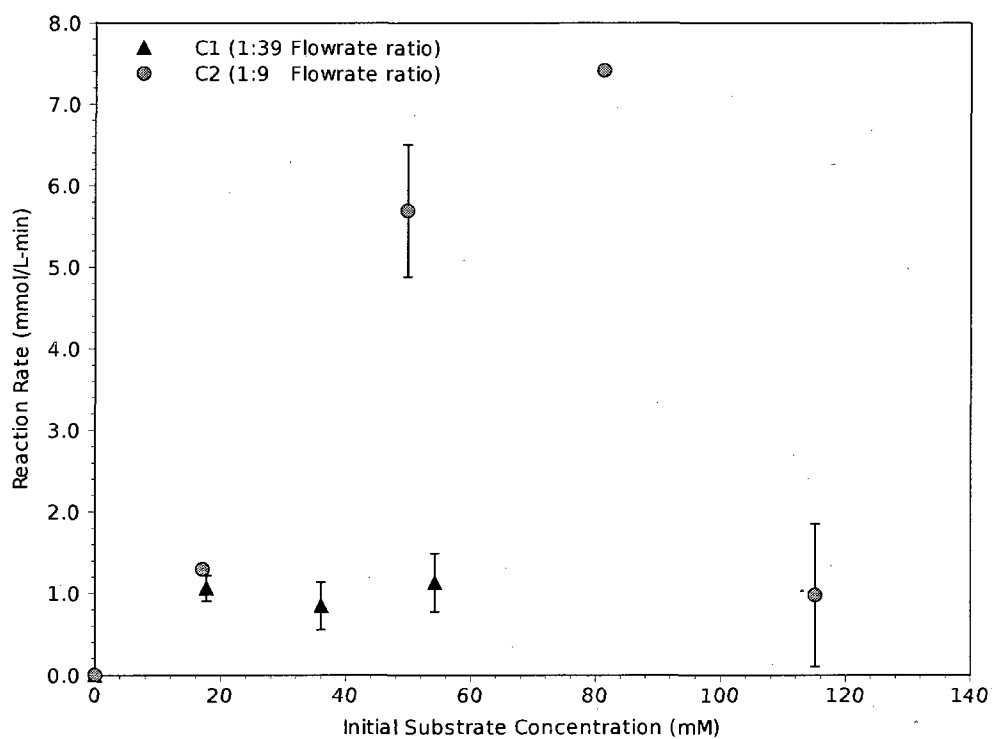


Figure 4-16: Average reaction rate as a function of initial substrate concentration for carrier-free enzyme aggregate reaction conditions shown in Table 3.5.

CHAPTER 5

SUMMARY AND FUTURE WORK

The fabrication of microdevices and their use as microscale multistep reactors provides many challenges. In this research, soft lithography techniques were developed to fabricate microchannels in PDMS layers. These layers were sealed using plasma treatment and interfaced with macroscale equipment to flow fluids through the microdevices. This provided a platform to explore the challenges of implementing assays on the microscale.

Fabrication provided challenges in nearly every step. High resolution photomasks were important in creating microchannels with smoother, more vertical sidewalls. 20,000 dpi photomasks were shown to yield better results than 5,000 dpi photomasks. UV exposure time, post-exposure baking time, and post-exposure baking temperature all contributed significantly to the quality of the resulting master mold. Rotation of the silicon wafer during the UV exposure step was important in controlling the width of the fabricated microchannels. The UV lamp probably did not generate a very collimated beam resulting in fabricated channel dimensions $\sim 1.5 - 3$ times larger than the design dimensions. Layer sealing and device interfacing were both

important challenges to overcome. Oxygen plasma treatment followed by baking under a weighted uniform surface for 2 – 3 hours was determined to be the most successful method of sealing PDMS layers. The most consistent results for interfacing with macroscale devices were observed when PDMS layers were cast with stainless steel tubing to pre-form inlet and outlet ports. These pre-formed ports were sized to be slightly smaller in diameter than the final tubing used for interfacing. The flexibility of the PDMS allowed the use of slightly larger tubing in a smaller diameter port and this slight compression also created a strong conformal seal which prevented leaks.

Flow experiments were conducted in the microdevices to study the decomposition of hydrogen peroxide by bovine liver catalase at low substrate concentrations. The reaction was first conducted by mixing a free catalase solution and substrate solution at a junction within the device at two concentrations of enzyme solution. The average reaction rate increased with the initial substrate concentration, reached a maximum and then dropped at higher initial substrate concentrations. The initial substrate concentration at which the maximum average reaction rate occurred was ~ 80 mmol/L which is consistent with macroscale batch reactions. The average reaction rate data at low initial substrate concentrations showed similar trends to a model scheme of a plug flow reactor followed by a fed batch reactor. However, due to the limitations of the experimental set up, the kinetic parameters could not be calculated.

Enzyme immobilization efforts focused on covalent binding of the enzyme to the microdevice wall. The method used in this research consisted of surface treatment

to reduce PDMS hydrophobicity followed by a silanization step. This prepared the surface for treatment with glutaraldehyde followed by exposure to the enzyme. Plasma and liquid phase oxidation of the PDMS variations were examined as well as variation of solvent, concentration, and treatment time for the silanizing agent, glutaraldehyde, and enzyme exposure steps. The average reaction rate data obtained from this study showed no specific dependence on the initial substrate calculations. Based on experiments and analysis of enzyme loading, we concluded that for all variations used, enzyme leached from the channel walls.

Finally, carrier-free immobilization of catalase was accomplished by forming enzyme aggregate particles using enzyme precipitation followed by binding with glutaraldehyde. These particles were filtered to isolate the $< 30\mu m$ fraction for use in microdevices. Activity was tested by batch reaction in a glass vial prior to use in microchannel flow experiments for two choices of precipitant. It was observed that enzyme aggregates fabricated with diglyme as a precipitant showed far greater activity than enzyme aggregates fabricated with acetone as precipitant. Flow experiments with carrier-free enzyme aggregate particles showed average reaction rate dependence on initial substrate concentration similar to free enzyme reactions and the series reactor model developed.

The results of this research provide several areas of improvement and suggestions for future study.

- A better control of fabricated width of the microchannel as compared to the design width is needed. To this end, a UV lamp source with a collimated beam should be used.

- Mixing within microchannels must be improved to reduce any stratification of flow with multiple fluid streams.
- Improvements in the quenching schemes would allow for a finer control over reaction times and allow for accurate measurements of kinetic parameters for the microscale enzymatic reactions.
- Studies using alternate techniques for carrier-bound enzyme immobilization may be useful in working toward the goal of a multistep microchannel reactor. Reduction or elimination of enzyme leaching is important in creating a functional microscale flow reactor that can be studied and characterized.
- Careful control of channel height and width in combination with selective filtration could be used to create a flow system in which the aggregate particle is slightly smaller than the channel size. Separation of aggregate particles from the reaction solution provides the opportunity for reuse. Methods for particle recovery from microdevices can be explored for use in these systems.

REFERENCES

- [1] Microchem datasheet for su-8 developer.
- [2] Ş. Akkuş Çetinus, Öztop, H.N., Immobilization of catalase on chitosan film, *Enzyme and microbial technology* 26 (7) (2000) 497–501.
- [3] Alptekin, Ö., Tükel Seyhan, S., Y. Deniz, Immobilization and characterization of bovine liver catalase on eggshell, *Journal of the Serbian Chemical Society* 73 (6) (2008) 609–618.
- [4] A. Bange, H. Halsall, W. Heineman, Microfluidic immunosensor systems, *Biosensors and Bioelectronics* 20 (12) (2005) 2488–2503.
- [5] G. Briggs, J. Haldane, A note on the kinetics of enzyme action, *Biochemical journal* 19 (2) (1925) 338–339.
- [6] B. Chance, A. Maehly, Assay of catalases and peroxidases, *Methods Enzymol* 2 (1955) 764–775.
- [7] N. Duran, E. Esposito, Potential applications of oxidative enzymes and phenoloxidase-like compounds in wastewater and soil treatment: a review, *Applied Catalysis B, Environmental* 28 (2) (2000) 83–99.
- [8] S. Ekstrom, P. Onnerfjord, J. Nilsson, M. Bengtsson, T. Laurell, G. Marko-Vargas, Integrated microanalytical technology enabling rapid and automated protein identification, *Anal. Chem* 72 (2) (2000) 286–293.
- [9] E. Eteshola, D. Leckband, Development and characterization of an ELISA assay in PDMS microfluidic channels, *Sensors & Actuators: B. Chemical* 72 (2) (2001) 129–133.
- [10] I. Fita, A. Silva, M. Murthy, M. Rossmann, The refined structure of beef liver catalase at 2.5 Å resolution, *Acta Crystallographica Section B: Structural Science* 42 (5) (1986) 497–515.
- [11] A. Fu, C. Spence, A. Scherer, F. Arnold, S. Quake, A microfabricated fluorescence-activated cell sorter, *Nature biotechnology* 17 (11) (1999) 1109–1111.
- [12] D. Goodsell, Catalase, doi: 10.2210/rcsb_pdb/mom_2004.9 (September 2004).
- [13] Z. Han, W. Li, Y. Huang, B. Zheng, Measuring Rapid Enzymatic Kinetics by Electrochemical Method in Droplet-Based Microfluidic Devices with Pneumatic Valves, *Analytical Chemistry* 81 (14) (2009) 5840–5845.

- [14] C. Hansen, E. Skordalakes, J. Berger, S. Quake, A robust and scalable microfluidic metering method that allows protein crystal growth by free interface diffusion, *Proceedings of the National Academy of Sciences* 99 (26) (2002) 16531–16536.
- [15] F. Hasan, A. Shah, A. Hameed, Industrial applications of microbial lipases, *Enzyme and Microbial Technology* 39 (2) (2006) 235–251.
- [16] K. Kanno, H. Kawazumi, M. Miyazaki, H. Maeda, M. Fujii, Enhanced enzymatic reactions in a microchannel reactor, *Australian journal of chemistry* 55 (11) (2002) 687–690.
- [17] M. Kerby, R. Legge, A. Tripathi, Measurements of kinetic parameters in a microfluidic reactor, *Anal. Chem* 78 (24) (2006) 8273–8280.
- [18] O. Kirk, T. Borchert, C. Fuglsang, Industrial enzyme applications, *Current opinion in biotechnology* 13 (4) (2002) 345–351.
- [19] O. Lardinois, M. Mestdagh, P. Rouxhet, Reversible inhibition and irreversible inactivation of catalase in presence of hydrogen peroxide, *Biochimica et Biophysica Acta (BBA)/Protein Structure and Molecular Enzymology* 1295 (2) (1996) 222–238.
- [20] V. Linder, E. Verpoorte, N. de Rooij, H. Sigrist, W. Thormann, Application of surface biopassivated disposable poly (dimethylsiloxane)/glass chips to a heterogeneous competitive human serum immunoglobulin G immunoassay with incorporated internal standard, *Electrophoresis* 23 (5) (2002) 740–749.
- [21] H. Lineweaver, D. Burk, The determination of enzyme dissociation constants, *Journal of the American Chemical Society* 56 (3) (1934) 658–666.
- [22] O. Loew, A new enzyme of general occurrence in organisms., *Science* 11 (279) (1900) 701–702.
- [23] T. Logan, D. Clark, T. Stachowiak, F. Svec, J. Frechet, Photopatterning enzymes on polymer monoliths in microfluidic devices for steady-state kinetic analysis and spatially separated multi-enzyme reactions, *Anal. Chem* 79 (17) (2007) 6592–6598.
- [24] H. Mao, T. Yang, P. Cremer, Design and characterization of immobilized enzymes in microfluidic systems, *Anal. Chem* 74 (2) (2002) 379–385.
- [25] J. Marshall, M. Rabinowitz, Stabilization of catalase by covalent attachment to dextran Synthetic Glycoproteins, Part V. See ref. 1 for Part IV., *Biotechnology and Bioengineering* 18 (9) (1976) 1325–1329.
- [26] M. Miyazaki, T. Honda, H. Yamaguchi, M. Briones, H. Maeda, Enzymatic processing in microfluidic reactors, *Biotechnology and Genetic Engineering Reviews* 25 (2008) 405–428.

- [27] M. Murthy, T. Reid 3rd, A. Sicignano, N. Tanaka, M. Rossmann, Structure of beef liver catalase., *Journal of molecular biology* 152 (2) (1981) 465–499.
- [28] A. Nomura, S. Shin, O. Mehdi, J. Kauffmann, Preparation, characterization, and application of an enzyme-immobilized magnetic microreactor for flow injection analysis, *Anal. Chem* 76 (18) (2004) 5498–5502.
- [29] J. Rogers, R. Nuzzo, Recent progress in soft lithography, *Materials today* 8 (2) (2005) 50–56.
- [30] A. Schmid, J. Dordick, B. Hauer, A. Kiener, M. Wubbolts, B. Witholt, Industrial biocatalysis today and tomorrow, *Nature* 409 (2001) 258–268.
- [31] R. Schoevaart, M. Wolbers, M. Golubovic, M. Ottens, A. Kieboom, F. Van Rantwijk, L. Van der Wielen, R. Sheldon, Preparation, optimization, and structures of cross-linked enzyme aggregates (CLEAs), *Biotechnology and bioengineering* 87 (6) (2004) 754–762.
- [32] G. Seong, J. Heo, R. Crooks, Measurement of enzyme kinetics using a continuous-flow microfluidic system, *Anal. Chem* 75 (13) (2003) 3161–3167.
- [33] R. Sheldon, Enzyme immobilization: the quest for optimum performance, *Advanced Synthesis & Catalysis* 349 (2007) 1289–1307.
- [34] R. Sheldon, R. Schoevaart, L. Van Langen, Cross-linked enzyme aggregates (CLEAs): A novel and versatile method for enzyme immobilization (a review), *Biocatalysis and Biotransformation* 23 (3) (2005) 141–147.
- [35] S. Sia, G. Whitesides, Microfluidic devices fabricated in poly (dimethylsiloxane) for biological studies, *Electrophoresis* 24 (21) (2003) 3563–3576.
- [36] H. Song, J. Tice, R. Ismagilov, A microfluidic system for controlling reaction networks in time., *Angewandte Chemie (International ed. in English)* 42 (7) (2003) 768–772.
- [37] A. Srinivasan, H. Bach, D. Sherman, J. Dordick, Bacterial P450-catalyzed polyketide hydroxylation on a microfluidic platform, *Biotechnology and bioengineering* 88 (4) (2004) 528–535.
- [38] A. Stroock, S. Dertinger, A. Ajdari, I. Mezic, H. Stone, G. Whitesides, Chaotic mixer for microchannels, *Science* 295 (5555) (2002) 647–651.
- [39] G. Sui, J. Wang, C. Lee, W. Lu, S. Lee, J. Leyton, A. Wu, H. Tseng, Solution-phase surface modification in intact poly (dimethylsiloxane) microfluidic channels, *Anal. Chem* 78 (15) (2006) 5543–5551.
- [40] J. Sumner, A. Dounce, Crystalline catalase, *Journal of Biological Chemistry* 121 (2) (1937) 417–424.

- [41] J. Switala, P. Loewen, Diversity of properties among catalases, *Archives of Biochemistry and Biophysics* 401 (2002) 145–154.
- [42] M. Thomsen, Pölt, P., B. Nidetzky, Development of a microfluidic immobilised enzyme reactor, *Chemical Communications* 2007 (24) (2007) 2527–2529.
- [43] I. Tinoco Jr., K. Sauer, J. Wang, J. Puglisi, *Physical Chemistry: Principles and Applications in Biological Sciences*, Prentice-Hall, Inc., 2003.
- [44] S. Tukel, O. Alptekin, Immobilization and kinetics of catalase onto magnesium silicate, *Process Biochemistry* 39 (12) (2004) 2149–2155.
- [45] P. Vasudevan, R. Weiland, Studies on the morphology of immobilized catalase, *Chemical engineering journal and the biochemical engineering journal* 55 (1-2) (1994) 41–45.
- [46] G. Walsh, *Proteins: Biochemistry and Biotechnology*, Wiley, 2002.
- [47] J. Wang, On the detailed mechanism of a new type of catalase-like action, *Journal of the American Chemical Society* 77 (18) (1955) 4715–4719.
- [48] G. Whitesides, E. Ostuni, S. Takayama, X. Jiang, D. Ingber, Soft lithography in biology and biochemistry, *Annual Review of Biomedical Engineering* 3 (1) (2001) 335–373.
- [49] L. Wilson, L. Betancor, G. Fernandez-Lorente, M. Fuentes, A. Hidalgo, J. Guisan, B. Pessela, R. Fernandez-Lafuente, Cross-linked aggregates of multimeric enzymes: a simple and efficient methodology to stabilize their quaternary structure, *Biomacromolecules* 5 (3) (2004) 814–817.
- [50] Y. Xia, G. Whitesides, Soft lithography, *Annual Review of Materials Science* 28 (1) (1998) 153–184.
- [51] S. Xie, F. Svec, J. Fréchet, Design of reactive porous polymer supports for high throughput bioreactors: Poly (2-vinyl-4, 4-dimethylazlactone-co-acrylamide-co-ethylene dimethacrylate) monoliths, *Biotechnology and bioengineering* 62 (1) (1999) 30–35.
- [52] B. Zheng, J. Tice, R. Ismagilov, Formation of arrayed droplets by soft lithography and two-phase fluid flow, and application in protein crystallization, *Advanced materials (Deerfield Beach, Fla.)* 16 (15) (2004) 1365–1368.

Appendix A

Microchem Datasheet for SU-8 Developer [1]
www.microchem.com/products/pdf/SU8_2035-2100.pdf



NANO™ SU-8 2000

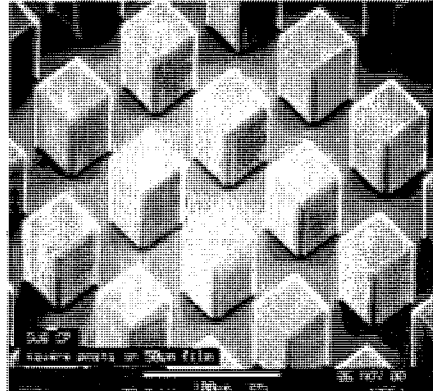
Negative Tone Photoresist Formulations 2035-2100

- High aspect ratio imaging
Near vertical side walls
- Near UV (350-400nm) processing
- Improved coating properties
Uniformity (lower surface tension)
Adhesion
- Faster drying
Improved throughput

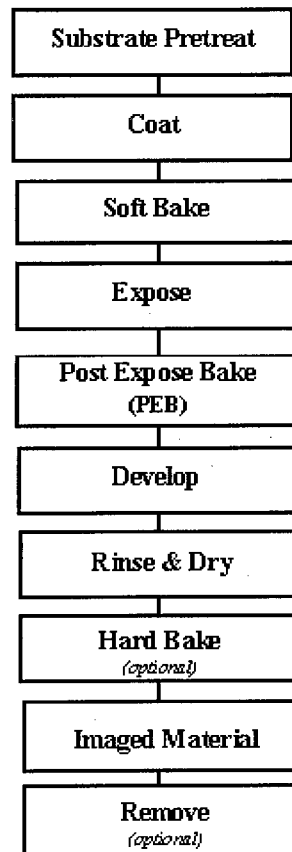
SU 8 2000 is a high contrast, epoxy based photoresist designed for micromachining and other microelectronic applications, where a thick, chemically and thermally stable image is desired. SU 8 2000 is an improved formulation of SU 8, which has been widely used by MEMS producers for many years. By using a faster drying, more polar solvent system, improved coating properties and higher throughput are realized. Film thicknesses of 0.5 to >200µm can be achieved with a single coat process. The excellent imaging characteristics of SU 8 are maintained. The exposed and subsequently cross linked portions of the film are rendered insoluble to liquid developers. SU 8 2000 has very high optical transparency above 360nm, which makes it ideally suited for imaging near vertical sidewalls in very thick films. SU 8 2000 is best suited for permanent applications where it is imaged, cured and left in place.

Process Guidelines

SU 8 2000 is most commonly processed with conventional near UV (350-400nm) radiation, although it may be imaged with e beam or x ray. i line (365nm) is recommended. Upon exposure, cross linking proceeds in two steps (1) formation of a strong acid during the exposure process, followed by (2) acid initiated, thermally driven epoxy cross linking during the post exposure bake (PEB) step.



Square posts in thick SU-8 2000



A normal process is: spin coat, soft bake, expose, post-expose bake (PEB) followed by develop. A controlled hard bake is recommended to further cross-link the imaged SU-8 2000 structures when they will remain as part of the device. The entire process should be optimized for the specific application. A baseline process is given here to be used as a starting point.

Substrate Pretreat

To obtain maximum process reliability, substrates should be clean and dry prior to applying the SU-8 2000 resist. Start with a solvent cleaning, or a rinse with dilute acid, followed by a DI water rinse. Where applicable, substrates should be subjected to a piranha etch / clean (H_2SO_4 & H_2O_2). To dehydrate the surface, bake at 200°C for 5 minutes on a contact hot plate or 30 minutes in a convection oven. Adhesion promoters are typically not required. For applications that require electroplating and subsequent removal of SU-8 2000 apply MicroChem's OmniCoat prior to processing.

Coat

SU-8 2000 resists are designed to produce low defect coatings over a very broad range of film thickness. The film thickness versus spin speed data displayed in Table 1 and Figure 1 provide the information required to select the appropriate SU-8 2000 resist and spin conditions, to achieve the desired film thickness.

The recommended coating conditions are:

- (1) STATIC Dispense: Approximately 1ml of SU-8 2000 per inch of substrate diameter.
- (2) Spread Cycle: Ramp to 500 rpm at 100 rpm/second acceleration. Hold at this speed for 5-10 seconds to allow the resist to cover the entire surface.
- (3) Spin Cycle: Ramp to final spin speed at an acceleration of 300 rpm/second and hold for a total of 30 seconds.

Product Name	Viscosity (cSt)	Thickness (µm)	Spin Speed (rpm)
		35	3000
SU-8 2035	7000	55	2000
		110	1000
		50	3000
SU-8 2050	14000	75	2000
		165	1000
		75	3000
SU-8 2075	22000	110	2000
		225	1000
		100	3000
SU-8 2100	45000	140	2000
		260	1000

Table 1. Thickness vs. spin speed data for selected SU-8 2000 resists.

** Approximate

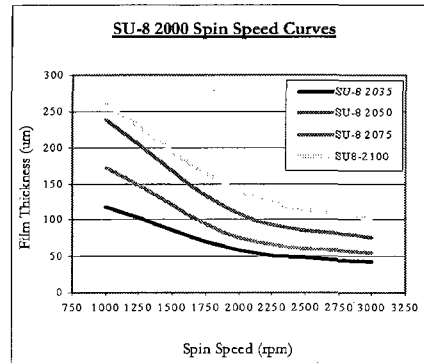


Figure 1. Spin speed vs. thickness curves for selected SU-8 2000 resists.

Soft Bake

After the resist has been applied to the substrate, it must be soft baked to evaporate the solvent and densify the film. SU-8 2000 is normally baked on a level hot plate, although convection ovens may be used. The following bake times are based on contact hot plate processes. Bake times should be optimized for proximity and convection oven bake processes since solvent evaporation rate is influenced by the rate of heat transfer and ventilation.

For best results, ramping or stepping the soft bake temperature is recommended. Lower initial bake temperatures allow the solvent to evaporate out of the film at a more controlled rate, which results in better coating fidelity, reduced edge bead and better resist-to-substrate adhesion. Refer to Table 2. for TWO STEP contact hot plate process recommendations.

Product Name	Thickness (µm)	Pre-bake @ 65° C	Softbake @ 95° C
	35	2	5
SU-8 2035	55	3	6
	110	5	20
	50	3	6
SU-8 2050	75	3	9
	165	5	30
	75	3	9
SU-8 2075	110	5	20
	225	5	45
	100	5	20
SU-8 2100	140	5	35
	260	7	60

Table 2. Recommended soft bake parameters

Expose

SU-8 is optimized for near UV (350-400nm) exposure. i-line exposure tools are recommended. SU-8 is virtually transparent and insensitive above 400nm but has high actinic absorption below 350nm. This can be seen in Figure 2. Excessive dose below 350nm may, therefore, result in over exposure of the top portion of the resist film, resulting in exaggerated negative sidewall profiles or T-topping. The optimal exposure dose will depend on film thickness (thicker films require higher dosage) and process parameters. The exposure dose recommendations in Table 3. are based on source intensity measurements taken with an i-line (365nm) radiometer and probe.

Expose tip: When using a broad spectral output source, for best imaging results, i.e. straightest sidewalls, filter out excessive energy below 350nm.

Catastrophic adhesion failure, severely negative sidewalls and excessive cracking often indicate an under cross-linking condition. To correct the problem, increase the exposure dose and/or increase the post exposure bake (PEB) time.

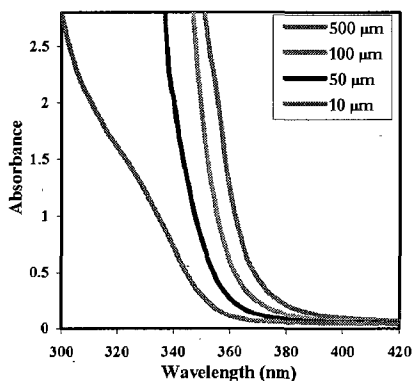


Figure 2. SU-8 absorbance vs. film thickness

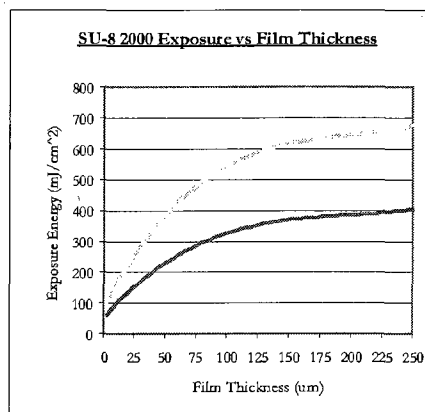


Table 3. Recommended expose dose processes

Post Expose Bake

Following exposure, a post expose bake (PEB) must be performed to selectively cross-link the exposed portions of the film. This bake can be performed either on a hot plate or in a convection oven. Optimum cross-link density is obtained through careful adjustments of the exposure and PEB process conditions. The bake recommendations below are based on results obtained with a contact hot plate.

PEB tip: SU-8 is readily cross-linked and can result in a highly stressed film. To minimize stress, wafer bowing and resist cracking, a slow ramp or TWO STEP contact hot plate process, as shown in Table 4., is recommended. Rapid cooling after PEB should be avoided.

Product Name	Thickness (μms)	PEB 1 @65°C	PEB 2 @95°C
SU-8 2035	35	1	3
	55	1	5
	110	1	10
SU-8 2050	50	1	5
	75	1	7
	165	1	12
SU-8 2075	75	1	7
	110	1	10
	225	1	15
SU-8 2100	100	1	10
	140	1	15
	260	1	15

Table 4. Recommended post expose bake parameters

Develop

SU-8 2000 resists have been optimized for use with MicroChem's SU-8 Developer. Immersion, spray or spray-puddle processes can be used. Other solvent based developers such as ethyl lactate and diacetone alcohol may also be used. Strong agitation is recommended for high aspect ratio and/or thick film structures. Recommended develop times are given in Table 5. for immersion processes. These proposed develop times are approximate, since actual dissolution rates can vary widely as a function of agitation rate, temperature and resist processing parameters.

Product Name	Thickness (μms)	Development (minutes)
	35	5
SU-8 2035	55	6
	110	10
	50	6
SU-8 2050	75	7
	165	12
	75	7
SU-8 2075	110	10
	225	12
	100	10
SU-8 2100	140	15
	260	20

Table 5. Recommended develop processes

Rinse and Dry

Following development, the substrate should be rinsed briefly with isopropyl alcohol (IPA), then dried with a gentle stream of air or nitrogen.

Rinse tip: If a white film is produced during rinse, this is an indication that the substrate has been under developed. Simply immerse or spray the substrate with SU-8 developer to remove the film and complete the development process. Repeat the rinse step.

Hard Bake (cure)

SU-8 2000 has good mechanical properties, therefore hard bakes are normally not required. For applications where the imaged resist is to be left as part of the final device, the resist may be ramp/step hard baked between 150-200°C on a hot plate or in a convection oven to further cross link the material. Bake times vary based on type of bake process and film thickness.

Removal

SU-8 2000, after expose and PEB, is a highly cross-linked epoxy, which makes it extremely difficult to remove with

conventional solvent based resist strippers. MicroChem's Remover PG will swell and lift off minimally cross-linked SU-8 2000. However, if OmniCoat has been applied immersion in Remover PG should effect a clean and thorough Lift-Off of the SU-8 2000 Material. It will not remove fully cured or hard baked SU-8 2000 without the use of OmniCoat. Alternate removal processes include immersion in oxidizing acid solutions such as piranha etch / clean, plasma ash, RIE, laser ablation and pyrolysis.

To remove minimally cross-linked SU-8 2000, or if using Omnicoat, with Remover PG, heat the bath to 50-80°C and immerse the substrates for 30-90 minutes. Actual strip time will depend on resist thickness and cross-link density. For more information on MicroChem Omnicoat and Remover PG please see the relevant product data sheets.

Storage

Store SU-8 2000 resists upright in tightly closed containers in a cool, dry environment away from direct sunlight at a temperature of 40-70°F(4-21°C). Store away from light, acids, heat and sources of ignition. Shelf life is twelve months from date of manufacture.

Disposal

SU-8 2000 resists may be included with other waste containing similar organic solvents to be discarded for destruction or reclaim in accordance with local state and federal regulations. It is the responsibility of the customer to ensure the disposal of SU-8 2000 resists and residues made in observance all federal, state, and local environmental regulations.

Environmental, Health and Safety

Consult product Material Safety Data Sheet before working with SU-8 2000 resists. Handle with care. Wear chemical goggles, chemical gloves and suitable protective clothing when handling SU-8 2000 resists. Do not get into eyes, or onto skin or clothing. Use with adequate ventilation to avoid breathing vapors or mist. In case of contact with skin, wash affected area with soap and water. In case of contact with eyes, rinse immediately with water and flush for 15 minutes lifting eyelids frequently. Get emergency medical assistance.

The information is based on our experience and is, we believe to be reliable, but may not be complete. We make no guarantee or warranty, expressed or implied, regarding the information, use, handling, storage, or possession of these products, or the application of any process described herein or the results desired, since the conditions of use and handling of these products are beyond our control.

MICRO-CHEM

1254 Chestnut Street
Newton, MA 02464

tel: (617)965-5511 fax: (617)965-5818

email: mcc@microchem.com www.microchem.com

Rev. 2/02